Trainability Enhancement of Parameterized Quantum Circuits via Reduced-Domain Parameter Initialization

Yabo Wang and Bo Qi*

Key Laboratory of Systems and Control, Academy of Mathematics and Systems Science, Chinese Academy of Sciences, Beijing 100190, P. R. China and University of Chinese Academy of Sciences, Beijing 100049, P. R. China

Chris Ferrie

Center for Quantum Software and Information, University of Technology Sydney, Ultimo NSW 2007, Australia

Daoyi Dong

School of Engineering and Information Technology, University of New South Wales, Canberra ACT 2600, Australia (Dated: February 15, 2023)

Parameterized quantum circuits (PQCs) have been widely used as a machine learning model to explore the potential of achieving quantum advantages for various tasks. However, the training of PQCs is notoriously challenging owing to the phenomenon of plateaus and/or the existence of (exponentially) many spurious local minima. In this work, we propose an efficient parameter initialization strategy with theoretical guarantees. It is proved that if the initial domain of each parameter is reduced inversely proportional to the square root of circuit depth, then the magnitude of the cost gradient decays at most polynomially as a function of the depth. Our theoretical results are verified by numerical simulations of variational quantum eigensolver tasks. Moreover, we demonstrate that the reduced-domain initialization strategy can protect specific quantum neural networks from exponentially many spurious local minima. Our results highlight the significance of an appropriate parameter initialization strategy and can be used to enhance the trainability of PQCs in variational quantum algorithms.

I. INTRODUCTION

A. Background

With the current noisy intermediate-scale quantum (NISQ) devices [1–3], a key and urgent question is whether we can exploit the potential power of NISQ devices to achieve quantum advantages in meaningful tasks [4–16]. To this end, variational quantum algorithms (VQAs) with parameterized quantum circuits (PQCs) have become a leading strategy [17–21].

VQAs are learning-based or optimization-based quantum-classical hybrid algorithms. The core idea is exploiting PQCs to delegate classically difficult computation and variationally updating the parameters in PQCs with a powerful classical optimizer [22–26]. With error mitigation techniques [27–31], VQAs have been applied to various fields and the corresponding specific algorithms have been developed, including variational quantum eigensolver (VQE) [32–35], quantum approximate optimization algorithm [12, 36–39], variational quantum simulator [40–43], quantum neural network (QNN) [44–54], and others [55–61].

Despite the success in many fields, VQAs still face many challenges when scaling up the size of PQCs. One of the key bottlenecks is the occurrence of barren plateaus

(BPs), which was first noticed in [62]. It was shown that for deep unstructured and randomly initialized PQCs, the magnitude of the gradient of the cost function corresponding to a single local operator decays exponentially with the number of qubits. Moreover, for any polynomial sum of local operators, the exponential decay of trainability cannot be circumvented. Thus, the occurrence of BPs prohibits PQCs from training in the very beginning unless exponentially many quantum resources are provided. In fact, BPs may arise in many scenarios, such as randomly initialized parameters, deep and problemagnostic PQCs [62–64], global cost function [65, 66], large expressibility [62, 67], entanglement [68, 69], and noise [70]. Moreover, the trainability issue cannot be addressed with gradient-free methods [71]. Thus, a solution or improvement is urgent for achieving potential quantum advantages.

In addition to the exponentially vanishing gradient, there is another bottleneck for training capability. For a wide class of under-parameterized variational quantum models, which are believed to exhibit no BP, the land-scapes of the cost function are generally swamped with spurious local minima and traps [72], and the quantities may exponentially depend on the number of parameters [73], which is extremely hard to optimize [74, 75].

^{*} qibo@amss.ac.cn

B. Related Work

In order to address the severe challenge of BPs, many strategies have been proposed. The main idea is to either design different circuit architectures or break the assumptions causing BPs.

Some constructed PQCs, such as tree tensor network [76, 77] and quantum convolutional neural network [50] can help avoid BPs, i.e, on average the gradient of cost function decays polynomially with the number of qubits [64, 78, 79]. However, due to their specific architectures, where the depth of the circuits is logarithmically versus the number of qubits, the gradient usually decays exponentially with the circuit depth instead. In addition, the expressive power of these PQCs may be limited even though the trainable parameters are drawn independently and identically from uniform distribution over the entire period $[-\pi, \pi]$.

On the other hand, ansatzes constructed in a probleminspired manner [69, 80–83] have been put forward to mitigate BPs, where the core idea is to reduce the unitary space explored. Moreover, in [43, 57], it was suggested that when the target Hamiltonian is a linear combination of unitaries one can circumvent the BP issue by constructing the ansatz in an iterative way. Ansatzes can also be trained layer-by-layer [84, 85], or designed by classical reinforcement learning [86].

Since BPs are cost function-dependent, it was suggested to encode the problem into local cost function, i.e., the expectation values of local observables [65]. The strategy works for circuits whose depths are logarithmic functions of the number of qubits N, but not for circuits whose depths are linear or polynomial functions of N [62, 65]. Moreover, the BPs cannot be mitigated for any polynomial sum of local operators.

Another practical viewpoint to address BPs is parameter initialization, which was highlighted in [39, 62, 67]. A heuristic initialization strategy was proposed in [87] with the purpose of limiting the effective depth of circuit, so that the parameter update is not stuck in a BP at the start of training. In [88], it was believed that correlated parameters in the ansatz can effectively reduce the parameter space and result in large gradients of cost function. A Bayesian learning initialization approach was employed in [89] to first identify a promising region in the parameter space and then employ the gradient-based or gradient-free optimizer for local search. Via simulations, [63] found an initial region of parameters that can improve the trainability and keep a high level of expressive power. A Gaussian initialization strategy was proposed with theoretical guarantees to escape from BPs in general deep circuits [90], where the lower bound of the norm of cost gradient decays at most polynomially with the circuit depth. Besides, for correlated parameterized gates, Gaussian initialization guarantees the update direction when training global observables which are generally believed to suffer from BPs even for very shallow circuits [90]. However, the theoretical or empirical results of the

above strategies for local observables are limited to single Pauli strings. For complex objectives corresponding to a summation of local Pauli strings, the trainability has yet to be investigated.

As for the training issue caused by the presence of many far from optimal persistent local minima or traps, it has been demonstrated that there is a connection between the over-parametrization onset and a phase transition of the trainability, where QNNs can be better trained [91–94]. However, the number of parameters needed for over-parametrization is comparable to the system size, that is, the circuit depth may be an exponential function of the number of qubits, which incurs unnecessary overhead and potential BPs.

C. Our Contributions

To address the trainability issue, we propose an efficient reduced-domain parameter initialization strategy. Our contributions are summarized as follows.

- For the cost function related to a summation of at most S-local Pauli operators, we theoretically prove that if the initial domain of each parameter in an L-depth circuit is reduced in proportion to $\frac{1}{\sqrt{L}}$, the norm of the gradient decays at most polynomially with L when the number of qubits N and the depth L increase. Thus, as L increases polynomially with N, VQAs are trainable in the beginning. The result is quite different from the belief that even with an S-local observable, BPs occur when L is a polynomial function of N.
- Via simulations, we also demonstrate that our parameter initialization strategy can protect QNNs from exponentially many spurious local minima in the cost function landscape. Compared with the over-parametrization strategy, our approach is not only economical on quantum resources, but also easily implementable in practice.

The paper is organized as follows. In Section II, we introduce the notation and describe the generic setup of VQAs. In Section III, we first present the theoretical results concerning the norm of the gradient of cost function under our reduced-domain parameter initialization strategy, and then extend the main results to the capacity of helping PQCs avoid BPs. In Section IV, via simulations we validate the theoretical results in VQE tasks, and generalize the reduced-domain initialization strategy to QNNs. Section V concludes the paper.

II. NOTATION AND SETUP OF VQAS

A. Quantum basics and notation

In quantum computing, information in an N-qubit system is described by quantum states which can be mathematically represented as a positive semi-definite Hermitian matrix $\rho \in \mathbb{C}^{2^N \times 2^N}$ with $\mathrm{Tr}(\rho) = 1$. If $\mathrm{rank}(\rho) = 1$, it is called a pure state; otherwise, it is mixed. A pure state can be represented in terms of a unit state vector $|\phi\rangle$ as $\rho = |\phi\rangle\langle\phi|$, where $\langle\phi| = |\phi\rangle^{\dagger}$. A mixed state can be regarded as a convex combination of pure states.

In quantum mechanics, a unitary operation U operating on a quantum state ρ behaves as $U\rho U^{\dagger}$, and is usually referred to as a gate in quantum circuit language. Typical single-qubit gates are rotations in terms of Pauli matrices:

$$R_X(\theta) = e^{-i\frac{\theta}{2}X}, \ R_Y(\theta) = e^{-i\frac{\theta}{2}Y}, \ R_Z(\theta) = e^{-i\frac{\theta}{2}Z},$$

where θ is the rotation angle, and Pauli matrices are denoted as

$$\sigma_0 = I = \begin{pmatrix} 1 & 0 \\ 0 & 1 \end{pmatrix}, \ \sigma_1 = X = \begin{pmatrix} 0 & 1 \\ 1 & 0 \end{pmatrix},$$
$$\sigma_2 = Y = \begin{pmatrix} 0 & -i \\ i & 0 \end{pmatrix}, \ \sigma_3 = Z = \begin{pmatrix} 1 & 0 \\ 0 & -1 \end{pmatrix}.$$

Moreover, the following three 2-qubit gates are widely employed to generate entanglement:

$$CZ = \begin{pmatrix} 1 & 0 & 0 & 0 \\ 0 & 1 & 0 & 0 \\ 0 & 0 & 1 & 0 \\ 0 & 0 & 0 & -1 \end{pmatrix}, CNOT = \begin{pmatrix} 1 & 0 & 0 & 0 \\ 0 & 1 & 0 & 0 \\ 0 & 0 & 0 & 1 \\ 0 & 0 & 1 & 0 \end{pmatrix},$$
$$i\sqrt{SWAP} = \begin{pmatrix} 1 & 0 & 0 & 0 \\ 0 & \frac{1}{\sqrt{2}} & \frac{i}{\sqrt{2}} & 0 \\ 0 & \frac{i}{\sqrt{2}} & \frac{1}{\sqrt{2}} & 0 \\ 0 & 0 & 0 & 1 \end{pmatrix}.$$

For convenience, denote by [n] the set $\{1, 2, \dots, n\}$, for any positive integer n. Let

$$\boldsymbol{\sigma_i} = \boldsymbol{\sigma_{(i_1, i_2, \dots, i_N)}} = \sigma_{i_1} \otimes \sigma_{i_2} \otimes \dots \otimes \sigma_{i_N}$$
 (1)

denote an N-qubit Pauli string, where $i_j \in \{0, 1, 2, 3\}$ for $j \in [N]$. For instance, we denote

$$Z_1 = \sigma_{(3,0,0,\cdots,0)} = Z \otimes I \otimes I \otimes \cdots \otimes I,$$

$$Z_1 Z_2 = \sigma_{(3,3,0,\cdots,0)} = Z \otimes Z \otimes I \otimes \cdots \otimes I.$$

Moreover, σ_i is said to be S-local if there are S non-identity components in the tensor product of Eq. (1), i.e., there are S nonzero elements in the vector $i = (i_1, i_2, \dots, i_N)$.

B. Setup of VQAs

VQAs provide a general framework for solving a wide range of problems. A typical VQA is comprised of basic elements: cost, ansatz, measurement, optimizer, and parameter initialization.

Cost: The first task of VQAs is to define an appropriate cost function which effectively encodes the problem to be solved. Without loss of generality, we consider the expectation value of an observable O as cost function in the form of

$$C(\boldsymbol{\theta}) = \text{Tr} \left[OU(\boldsymbol{\theta}) \rho U^{\dagger}(\boldsymbol{\theta}) \right].$$
 (2)

Here, ρ is the input state, and $U(\theta)$ denotes a parameterized quantum unitary with the parameter vector θ to be optimized. In VQAs, an implicit assumption is that the cost function should be classically computationally intensive and the value can be obtained by performing quantum measurements on a quantum circuit with possible classical post-processing.

In this work, we consider VQE tasks aiming at finding the least eigenvalue of a given Hamiltonian H. We choose $\rho = |0\rangle\langle 0|$ and set O = H in Eq. (2). In particular, we consider H as

$$H = \sum_{i \in \mathcal{N}} \sigma_i = \sum_{i \in \mathcal{N}} \sigma_{(i_1, i_2, \dots, i_N)}, \tag{3}$$

where \mathcal{N} is a subset of $\mathcal{N}_S = \{i = (i_1, i_2, \cdots, i_N) : 1 \leq \sum_{j=1}^{N} 1_{i_j \neq 0} \leq S\}$, and 1_{ω} is the indicator function of the event ω . That is, H is a sum of N-qubit Pauli strings with locality of at most S.

Ansatz: Another key element of VQAs is ansatz, i.e., PQC whose parameters are optimized to minimize the corresponding cost function. In this work, we consider a PQC similar to that in [90]. As illustrated in Fig. 1(a), it is comprised of L blocks, each of which is composed of an entanglement layer CZ_l including CZ gates on arbitrarily many qubit pairs and two layers of R_X and R_Y gates on all qubits. There are two widely used structures of the entanglement layer: the fully connected topology as shown in Fig. 1(b), and the nearest-neighbor pairs topology with closed boundary condition as shown in Fig. 1(c). It should be pointed out that our results do not rely on the specific topology of CZ_l and can also be generalized to other structures of PQC.

Measurement: In our VQE task, the Hamiltonian of interest is formulated in terms of Pauli strings. To obtain the value of cost function, we may efficiently implement measurement in the Z basis on at most S qubits each time to evaluate the expectation value of each individual term in Eq. (3) and then sum up them.

Optimizer: The core task of the classical processor is updating the parameters to minimize the cost. Under the structure of the PQC illustrated in Fig. 1(a), the analytical gradient can be calculated on quantum hardwares by utilizing the parameter-shift rule [95–97]. In this work,

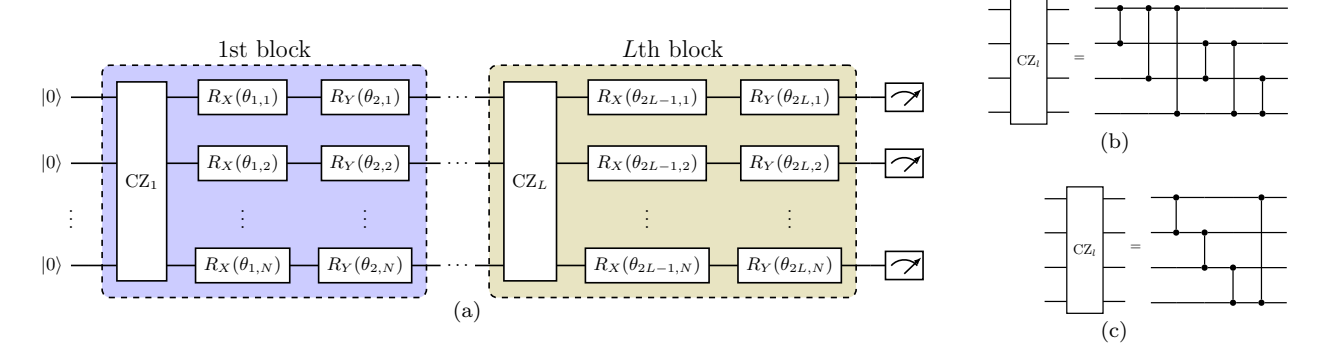


FIG. 1. Setup of ansatz. (a) PQC for VQE tasks. It consists of L blocks, each of which is comprised of three parts. Specifically, in the lth block, we first perform the entanglement layer CZ_l composed of arbitrarily many CZ gates, and then successively perform R_X gate and R_Y gate on each qubit. (b) CZ_l layer with the fully connected topology. (c) CZ_l layer with the nearest-neighbor pairs topology and the closed boundary condition.

we aim to analyze the norm of the gradient which greatly impacts the trainability of VQAs.

Parameter initialization: Due to the possibility of occurrence of BPs and/or the existence of exponentially many spurious local minima when training VQAs, it is critical to find an appropriate parameter initialization strategy to enhance the trainability.

For the PQC illustrated in Fig. 1(a), there are 2L layers of parameterized rotation gates with 2NL variational parameters in total, denoted by

$$\boldsymbol{\theta} = \boldsymbol{\theta}_{[2L]} = (\boldsymbol{\theta}_1, \boldsymbol{\theta}_2, \cdots, \boldsymbol{\theta}_{2L}),$$

where $\theta_q = (\theta_{q,1}, \theta_{q,2}, \cdots, \theta_{q,N})$ denotes the vector of rotation angles in the qth layer for $q \in [2L]$. To be specific, for the lth block, $l \in [L]$, and the jth qubit, $j \in [N]$, $\theta_{2l-1,j}$ denotes the rotation angle around X, while $\theta_{2l,j}$ denotes that around Y.

III. MAIN RESULTS

In previous works, the initial parameters are usually drawn independently and identically from a uniform distribution over an entire period $[-\pi, \pi]$, and the N-qubit local observable is always chosen as a simple Pauli string, for instance, Z_1Z_2 . For example, under a PQC similar to ours, [62] demonstrated that a BP occurs even when the depth L is a modest linear function, that is, L=10N, and the exponential decay cannot be circumvented for any polynomial sum of these local operators. For the simple observable Z_1Z_2 , [63] numerically showed that the trainability can be improved if each parameter is randomly chosen from $[-a\pi, a\pi]$. The satisfying value of a was identified by searching from 10^{-10} to 1 via simulations.

In this work, we consider a general Hamiltonian in the form of Eq. (3), where the number of individual terms in the summation can be arbitrary, including one. For the complex objective, we propose a reduced-domain parameter initialization strategy, in which each parameter

is independently and uniformly chosen from a reduced interval $[-a\pi, a\pi]$, where the hyperparameter a is depth-dependent and will be given in the following theorems.

In view of the setup in Section II, the decrease in the value of cost function after an update of the parameters can be quantified in terms of the magnitude of $\|\nabla_{\theta}C\|_{2}^{2}$ (see Appendix A). Thus, we adopt its average value $\mathbb{E}\|\nabla_{\theta}C\|_{2}^{2}$ as the trainability figure of merit.

Now we provide theoretical guarantees of the reduceddomain initialization strategy by establishing lower bounds on the norm of gradient at the first step.

Warm-up: We first consider a warm-up where the N-qubit Hamiltonian reads

$$H = \sum_{j=1}^{N-1} Z_j Z_{j+1}.$$
 (4)

For the ease of notation, denote

$$\alpha = \frac{1}{4} \left(2 + \frac{\sin 2a\pi}{a\pi} \right), \, \beta = \frac{1}{4} \left(2 - \frac{\sin 2a\pi}{a\pi} \right), \, \gamma = \frac{\sin a\pi}{a\pi}.$$

Theorem III.1. Consider the VQE problem, where the cost function is Eq. (2) with the Hamiltonian being Eq. (4), the ansatz illustrated as in Fig. 1(a), the initial state chosen as $\rho = |0\rangle\langle 0|$, and each parameter in $\boldsymbol{\theta}$ chosen from $[-a\pi, a\pi]$ independently and uniformly. Let $\nabla_{\boldsymbol{\theta}} C$ denote the gradient of the cost function with respect to $\boldsymbol{\theta}$. Then the average of the squared norm of the gradient is lower bounded by

$$\mathbb{E}_{\theta} \|\nabla_{\theta} C\|_{2}^{2} \ge 4(2N - 3)L\gamma^{8L - 2}\beta. \tag{5}$$

Furthermore, if the hyperparameter a is selected as

$$a = \frac{1}{4\pi} \sqrt{\frac{40L + 7 - \sqrt{1600L^2 - 400L + 49}}{L}} \in \Theta\left(\frac{1}{\sqrt{L}}\right),$$
(6)

then the gradient norm can be lower bounded by

$$\mathbb{E} \|\nabla_{\theta} C\|_{2}^{2} \ge e^{-1}(2N - 3), \tag{7}$$

where e is the natural constant.

For the local observable of Eq. (4), under the reduced-domain initialization strategy with the hyperparameter $a \in \Theta\left(\frac{1}{\sqrt{L}}\right)$, the trainability can be remarkably enhanced. Not only does the lower bound of the gradient norm not decrease when the circuit depth increases, but also it increases as the number of qubits increases. In particular, for the simple N-qubit observable Z_1Z_2 , the gradient norm can be lower bounded by a constant, which is quite different from the result in [62], where the gradient norm vanishes exponentially.

General case: Now we consider the general case with the N-qubit Hamiltonian in the form of Eq. (3).

Theorem III.2. Consider the VQE problem, where the cost function is Eq. (2) with the Hamiltonian being Eq. (3), the ansatz illustrated as in Fig. 1(a), the initial state chosen as $\rho = |0\rangle\langle 0|$, and each parameter in $\boldsymbol{\theta}$ chosen from $[-a\pi, a\pi]$ independently and uniformly. Let $\nabla_{\boldsymbol{\theta}} C$ denote the gradient of the cost function with respect to $\boldsymbol{\theta}$. Then the average of the squared norm of the gradient is lower bounded by

$$\mathbb{E}_{\mathbf{A}} \|\nabla_{\mathbf{\theta}} C\|_{2}^{2} \ge 2|\mathcal{N}|(L-1)\alpha^{2SL-1}\beta^{S+1}, \tag{8}$$

where $|\mathcal{N}|$ denotes the cardinality of the set \mathcal{N} .

Furthermore, if the hyperparameter a is selected as the solution of the following equation

$$\frac{\sin 2a\pi}{2a\pi} = \frac{S(2L-1)-2}{S(2L+1)},\tag{9}$$

where $a \in \Theta\left(\frac{1}{\sqrt{L}}\right)$, then the gradient norm can be lower bounded by

$$\mathbb{E}_{\theta} \|\nabla_{\theta} C\|_{2}^{2} \ge 2|\mathcal{N}| \left(\frac{S+1}{eS}\right)^{S+1} \frac{L-1}{(2L+1)^{S+1}}.$$
 (10)

From Theorem III.2, for VQE problems with Hamiltonian being a summation of a series of local Pauli strings, the trainability can be greatly enhanced by appropriately reducing the initial domain of parameters. Specifically, the lower bound of the gradient norm decays at most polynomially with the circuit depth. In addition, the lower bound increases linearly with the number of individual Pauli strings in the Hamiltonian, which guarantees the efficiency of the reduced-domain strategy for complex objectives.

The proofs of Theorems III.1 and III.2 are given in Appendix C and Appendix D, respectively. The basic idea is inspired by the proof of Theorem 4.1 in [90], where the observable considered is restricted to a single local Pauli string. However, in our work, the observables are in the form of a sum of local Pauli strings, so that we additionally need to deal with the cross terms generated from different strings when analyzing the norm of gradient. Specifically, we prove that under the selected initial

state, these cross terms are non-negative by analyzing the transformations of the involved Pauli strings after taking the expectations over the trainable parameters and applying the entanglement layers.

Avoiding BPs: We now extend the main results to the capacity of avoiding BPs.

In general, an N-qubit cost function C is said to exhibit a BP in the θ_v direction, if $\underset{\boldsymbol{\theta}}{\mathbb{E}} \partial_{\theta_v} C = 0$, and the variance decreases exponentially with N, that is,

$$\operatorname{\mathbb{V}ar}_{\boldsymbol{\theta}} \partial_{\theta_{v}} C \in O\left(b^{N}\right), \text{ for some } b \in (0,1).$$

On the other hand, it is said to be trainable, if the variance decreases polynomially with N, that is,

$$\operatorname{\mathbb{V}ar}_{\boldsymbol{\theta}} \partial_{\theta_v} C \in \Omega\left(\frac{1}{\operatorname{poly}(N)}\right).$$

Similarly, we can define circuit depth dependent BP, as the depth is also a key figure of merit in VQAs. The number of qubits and circuit depth are unified as the size of PQC.

The following theorems state that the reduced-domain parameter initialization strategy with a selected hyperparameter in the scaling of $\frac{1}{\sqrt{L}}$ can help PQCs avoid BPs. Remarkably, they hold for PQCs whose depths are polynomial functions of the number of qubits, while [62] demonstrated that for a wide class of randomly initialized PQCs of reasonably modest depth, BPs occur even with simple local operators.

Theorem III.3. Under the same assumptions as in Theorem III.1, let $\partial_{\theta_{q,n}}C$ denote the partial derivative of cost function with respect to $\theta_{q,n}$. For $q \in [2L]$ and $n \in [N]$, we have

$$\underset{\boldsymbol{\theta}}{\mathbb{E}} \, \partial_{\theta_{q,n}} C = 0, \tag{11}$$

and for $q \in [2L]$, the variance is lower bounded by

$$\operatorname{Var}_{\boldsymbol{\theta}} \partial_{\theta_{q,n}} C \ge f_n(L, a). \tag{12}$$

(i) For $n \in \{1, N\}$,

$$f_n(L, a) = \alpha^{4L - 1} \beta. \tag{13}$$

Furthermore, if the hyperparameter a is selected as the solution of the following equation

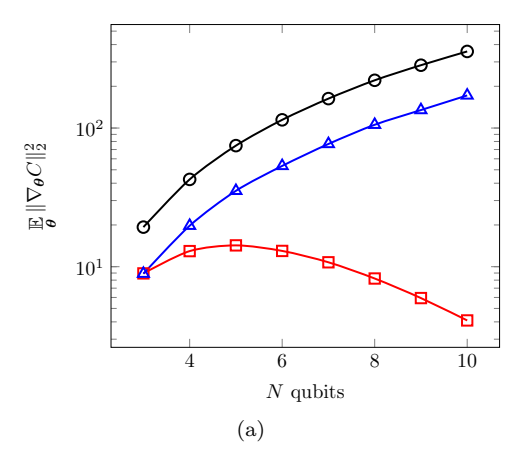
$$\frac{\sin a\pi}{a\pi} = \frac{2L - 1}{L},\tag{14}$$

where $a \in \Theta\left(\frac{1}{\sqrt{L}}\right)$, then we have

$$\operatorname{Var}_{\boldsymbol{\theta}} \partial_{\theta_{q,n}} C \ge \frac{1}{4eL}. \tag{15}$$

(ii) For $n \in \{2, 3, \dots, N-1\}$,

$$f_n(L, a) = 2\alpha^{4L-1}\beta + 2\gamma^{4L}\alpha^{2L-1}\beta.$$
 (16)



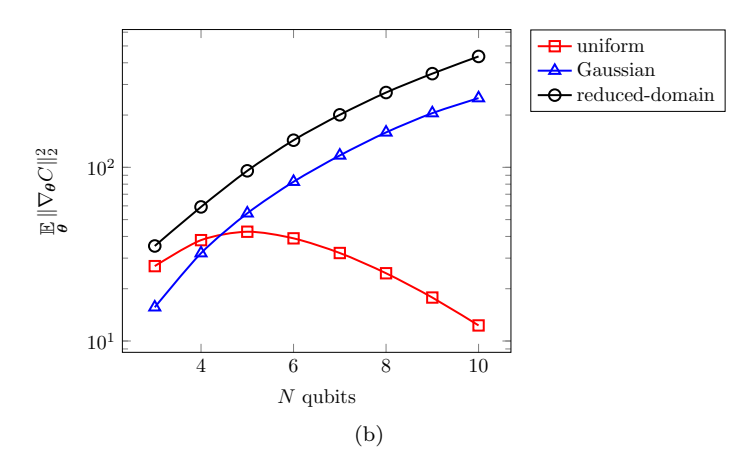


FIG. 2. The magnitudes of the mean squared norm of the cost function gradient at the first step versus the number of qubits under three initialization strategies: uniform (square), Gaussian (triangle), and reduced-domain (circle) on a semi-log plot. Here, S=2 and L=5N. The variance σ^2 in Gaussian initialization is chosen as $\frac{1}{8SL}=\frac{1}{80N}$. (a) The warm-up Hamiltonian case. (b) The Heisenberg Hamiltonian case. The hyperparameter a in the reduced-domain strategy is selected according to Eq. (6) or (9) for Hamiltonian of Eq. (4) or (22). In both cases, there exists a BP under uniform initialization, while the other two strategies help PQC avoid BPs with the gradient norms increasing exponentially with the qubit number N. It is clear that the reduced-domain strategy is superior to Gaussian initialization.

Furthermore, if the hyperparameter a is selected according to Eq. (6) in Theorem III.1, where $a \in \Theta\left(\frac{1}{\sqrt{L}}\right)$, then we have

$$\operatorname{Var}_{\boldsymbol{\theta}} \partial_{\theta_{q,n}} C \ge \frac{1}{eL}. \tag{17}$$

Theorem III.4. Under the same assumptions as in Theorem III.2, let $\partial_{\theta_q,n}C$ denote the partial derivative of cost function with respect to $\theta_{q,n}$. For $q \in [2L-2]$ and $n \in [N]$, the average of the squared norm of the partial derivative is lower bounded by

$$\mathbb{E}_{\boldsymbol{\theta}} \left(\partial_{\theta_{q,n}} C \right)^2 \ge \alpha^{2SL-1} \beta^{S+1}. \tag{18}$$

In addition, if for each $i \in \mathcal{N}$, the number of its elements belonging to the set $\{1,2\}$ is not equal to one, then we have

$$\underset{\boldsymbol{\theta}}{\mathbb{E}} \, \partial_{\theta_{q,n}} C = 0, \tag{19}$$

and the variance is lower bounded by

$$\operatorname{Var}_{\boldsymbol{\theta}} \partial_{\theta_{q,n}} C \ge \alpha^{2SL-1} \beta^{S+1}. \tag{20}$$

Furthermore, if the hyperparameter a is selected according to Eq. (9) in Theorem III.2, where $a \in \Theta\left(\frac{1}{\sqrt{L}}\right)$, we have

$$\mathbb{E}_{\boldsymbol{\theta}} \left(\partial_{\theta_{q,n}} C \right)^2 \ge \left(\frac{S+1}{eS} \right)^{S+1} \frac{1}{(2L+1)^{S+1}}. \tag{21}$$

IV. EXPERIMENTS

In this section, we validate the reduced-domain initialization strategy via two applications in VQAs, including VQE and QNN. All the experiments are run on Intel Core i7-11700K Processor (3.60GHz) with 16GB memory. We classically simulate the experiments by using the analytical form of the cost function and its gradient.

A. VQE

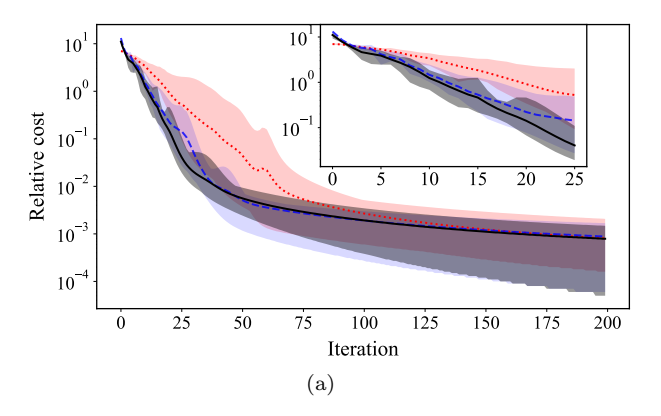
For VQE tasks, we investigate the N-qubit warm-up Hamiltonian of Eq. (4), whose ground energy is easy to calculate, and the N-qubit Heisenberg model

$$H = \sum_{i=1}^{N-1} X_i X_{i+1} + Y_i Y_{i+1} + Z_i Z_{i+1},$$
 (22)

whose ground energy becomes hard to obtain as N increases.

We adopt the ansatz illustrated in Fig. 1(a) and fix the entanglement layer in each block arranged in the nearest-neighbor pairs topology with closed boundary condition as shown in Fig. 1(c). For trainability and convergence, we compare three different parameter initialization strategies, including uniform distribution $\mathcal{U}[-\pi,\pi]$, Gaussian distribution $\mathcal{N}(0,\sigma^2)$ with the variance $\sigma^2 = \frac{1}{8SL}$ [90], and the reduced-domain distribution $\mathcal{U}[-a\pi,a\pi]$ with the hyperparameter a selected according to Eq. (6) or (9) corresponding to Hamiltonian of Eq. (4) or (22), respectively.

In Fig. 2, we compare the magnitudes of the mean squared norm of the gradient at the first step under the



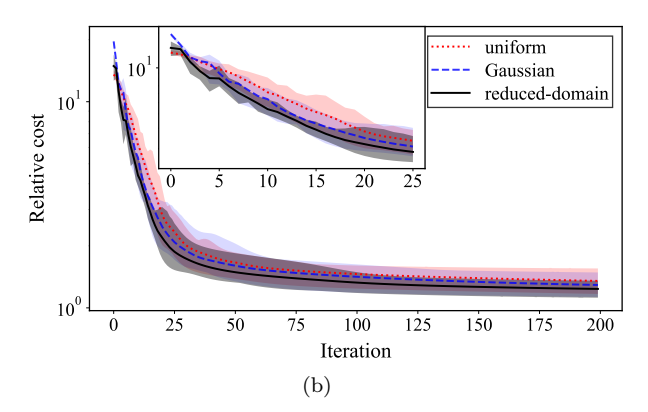


FIG. 3. The convergence behavior of the difference between the cost function value and the global minimum under uniform (dotted line), Gaussian (dashed line), and reduced-domain (solid line) initializations in the 8-qubit case on a semi-log plot. The insets show the trainability in the beginning iterations. Here, S=2 and L=8. The variance σ^2 in Gaussian initialization is chosen as $\frac{1}{8SL} = \frac{1}{128}$. (a) For the warm-up Hamiltonian, the hyperparameter a in the reduced-domain strategy is selected to be 0.0973 according to Eq. (6). The global minimum can be attained under all of the three strategies. (b) For the Heisenberg Hamiltonian, the hyperparameter a is selected to be 0.1685 according to Eq. (9). The global minimum cannot be achieved under all of the three strategies, while under the reduced-domain strategy, a smaller value can be attained in a faster way.

three initialization strategies. Here, S=2, and we set L=5N so that the PQC includes the same number of rotation layers 10N as that in Figure 3 of [62]. We depict the average points over 2500 rounds of experiments on a semi-log plot. From Fig. 2, under uniform initialization, the magnitude of the cost gradient decays exponentially as the number of qubits N increases, which coincides with both the theoretical and empirical results concerning BPs in [62]. In contrast, the magnitude of the gradient increases in an exponential way under the reduced-domain and Gaussian initialization. It is clear that the reduced-domain strategy outperforms Gaussian initialization.

We then adopt the relative cost, the difference between the cost function value and the global minimum, to evaluate the convergence behavior. Set L = N and N=8. The convergency behavior under the three initialization strategies are illustrated in Fig. 3 on a semi-log plot. Here, VQAs are trained using the accurate gradients with RMSProp, which performs like a speedy version of Adam. Although RMSProp and Adam naturally adapt their learning rates, it was shown in [98] that a learning rate multiplier schedule can substantially improve Adam's performance. Hence, we employ the learning rate η decreasing from 0.01 to 0.005 linearly with the ordinal of iterations during the training. The smoothing constant for mean-squared estimation is set as 0.999. We implement 10 rounds of experiments for each initialization strategy with 200 iterations for each round. Each line depicts the average behavior of the 10 rounds of experiments, while each filled area is the smallest area that includes the respective behaviors of the 10 rounds.

We notice that under the reduced-domain strategy, the relative cost converges faster. Furthermore, for the warm-up Hamiltonian of Eq. (4), global convergence can be achieved under all of the three strategies, as shown in Fig. 3(a). However, for more complicated Hamiltonians, for instance, Hamiltonian Eq. (22), global minimum is much harder to achieve under the PQC in Fig. 1(a). Although the reduced-domain parameter initialization strategy helps enhance trainability, much effort is needed for achieving global convergence.

B. QNN

We now extend the reduced-domain initialization strategy to QNN. In Proposition 5 of [73], it was demonstrated that in the under-parameterized region, there exists such a dataset that can induce a loss function with exponentially many spurious local minima. Subsequently, several simple yet extremely hard QNN instances for training were presented, where the initial parameters are independently drawn from the entire period. Here we focus on Example 2 in [73] to demonstrate that under the reduced-domain parameter initialization strategy, global convergence can be achieved.

Let us first briefly introduce the hard instance for training in [73]. There, the depth L=1, and for the p-parameter instance, their construction involves N=p qubits with the loss function $L(\theta)$ represented as

$$\frac{1}{2p} \sum_{l=1}^{p} \left[\left(\sin 2\theta_l - \sin \frac{\pi}{50} \right)^2 + \frac{1}{4} \left(\cos 2\theta_l - \cos \frac{\pi}{50} \right)^2 \right], \tag{23}$$

where the corresponding p-dimensional parameter vector is denoted by $\boldsymbol{\theta}=(\theta_1,\theta_2,\cdots,\theta_p)$. It was proved that there are 2^p minima within each period, for instance, $[-\frac{\pi}{2},\frac{\pi}{2}]$, where the global minimum is obtained at $\boldsymbol{\theta}^{\star}=\left(\frac{\pi}{100},\ldots,\frac{\pi}{100}\right)$, and the other 2^p-1 local minima are spurious with non-negligible suboptimality gap.

We follow the same routine as in [73], where QNNs are trained by using back-propagating gradients with RM-SProp. The constant learning rate is set to be 0.01, and the smoothing constant for mean-squared estimation is 0.99. We perform 5000 rounds of experiments with 200 iterations for each round.

In Fig. 4, we compare the relative frequencies of achieving global convergence under uniform initialization $\mathcal{U}\left[-\frac{\pi}{2},\frac{\pi}{2}\right]$ as in [73] and the reduced-domain strategy $\mathcal{U}\left[-a\frac{\pi}{2},a\frac{\pi}{2}\right]$, with a=0.1. From the semi-log plot, it is clear that under uniform initialization, the probability of success decays exponentially with the number of qubits (or parameters). In particular, in the 18-qubit case, there is no round achieving the global minimum within 5000 rounds of experiments. In contrast, under reduced-domain initialization, global convergence can always be achieved.

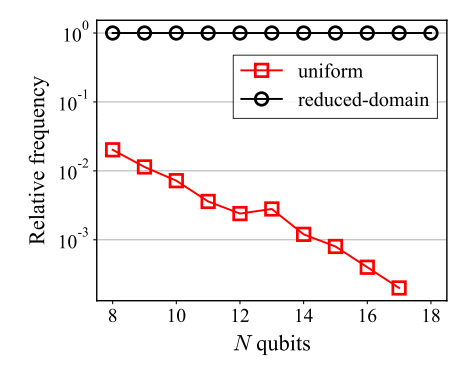


FIG. 4. The relative frequencies of achieving global convergence in 5000 rounds of experiments under uniform initialization (square) and reduced-domain initialization (circle) with the hyperparameter a=0.1 on a semi-log plot. Here, the missing point for uniform initialization in the 18-qubit case is owing to no round of success. The probability of success decays exponentially with the number of qubits under uniform initialization, while it is always 1 under the reduced-domain strategy.

To further demonstrate the efficiency of the reduced-domain initialization, we draw the initial parameters independently from the translational uniform distribution $\mathcal{U}\left[\frac{\pi}{4}-a\frac{\pi}{2},\frac{\pi}{4}+a\frac{\pi}{2}\right]$ with a=0.1. Remarkably, it can be verified that the global minimum $\boldsymbol{\theta}^*=\left(\frac{\pi}{100},\ldots,\frac{\pi}{100}\right)$ is outside of the reduced domain. We illustrate the distributions of the loss function value at convergence under reduced-domain initialization $\mathcal{U}\left[\frac{\pi}{4}-a\frac{\pi}{2},\frac{\pi}{4}+a\frac{\pi}{2}\right]$ and uniform initialization $\mathcal{U}\left[-\frac{\pi}{2},\frac{\pi}{2}\right]$ for the 16-qubit case in Fig. 5. For 5000 rounds of experiments, the cumulative frequency of global convergence is 2 for uniform initialization, while 5000 for reduced-domain initialization.

It is clear that under the reduced-domain strategy, it is more efficient and economical to obtain global convergence than the over-parametrization strategy.

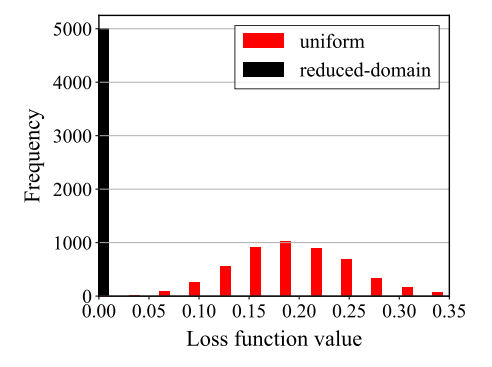


FIG. 5. The distributions of the loss function value at convergence for the 16-qubit case. For both the uniform $(\mathcal{U}\left[-\frac{\pi}{2},\frac{\pi}{2}\right])$ and reduced-domain $(\mathcal{U}\left[\frac{\pi}{4}-a\frac{\pi}{2},\frac{\pi}{4}+a\frac{\pi}{2}\right]$ with a=0.1) strategy, we implement 5000 rounds of experiments with 200 iterations for each round. The reduced-domain strategy achieves global convergence in all of the rounds, while the uniform one only succeeds twice.

V. CONCLUSION AND DISCUSSION

In this paper, we have presented an efficient reduceddomain parameter initialization strategy to enhance trainability of VQAs. For Hamiltonians represented as a sum of local Pauli strings, we have theoretically proved that with the reduced-domain strategy, the average of the squared norm of the cost gradient decays at most polynomially with the depth of circuit and increases linearly with the number of individual terms in the summation of Hamiltonian. Thus, it clearly implies that reduceddomain initialization helps PQC avoid the notorious phenomenon of BPs. Our empirical results have validated the theoretical results in VQE tasks. Moreover, via simulations, we have demonstrated that the reduced-domain strategy can also help address the poor convergence in presence of exponentially many spurious local minima in under-parameterized QNNs. The reduced-domain initialization strategy has the potential to significantly enhance trainability of PQCs and generate wide impact on developing algorithms with quantum advantages for various practical applications.

Appendix A: The norm of gradient

In this section, we explain the meaning of the figure of merit $\|\nabla_{\theta} C\|_{2}^{2}$.

In gradient-based optimizers, the parameter vector $\boldsymbol{\theta}$ updates as

$$\boldsymbol{\theta}_{t+1} = \boldsymbol{\theta}_t - \eta \nabla_{\boldsymbol{\theta}} C(\boldsymbol{\theta}_t),$$

where η denotes the learning rate, which is usually small. With the update, the value of cost function decreases as

$$C(\boldsymbol{\theta}_{t+1}) = C(\boldsymbol{\theta}_t - \eta \nabla_{\boldsymbol{\theta}} C(\boldsymbol{\theta}_t))$$

= $C(\boldsymbol{\theta}_t) - \eta \|\nabla_{\boldsymbol{\theta}} C(\boldsymbol{\theta}_t)\|_2^2 + o(\eta)$.

It is clear to see that the decrease with parameters updating is quantified in terms of the magnitude of $\|\nabla_{\theta}C\|_{2}^{2}$. Thus, we adopt the average $\mathbb{E}_{\theta} \|\nabla_{\theta}C\|_{2}^{2}$ as the trainability figure of merit.

Appendix B: Technical Lemmas

In this section, we present several technical lemmas, which are all based on the following assumption.

Assumption B.1. A random variable θ is drawn from uniform distribution over $[-a\pi, a\pi]$, where $a \in (0, 1)$ is a hyperparameter to be further determined.

Under the assumption, let \mathbb{E} denote the expectation over θ with respect to the uniform distribution $\mathcal{U}[-a\pi, a\pi]$. Recall that

$$\alpha = \frac{1}{4} \left(2 + \frac{\sin 2a\pi}{a\pi} \right), \, \beta = \frac{1}{4} \left(2 - \frac{\sin 2a\pi}{a\pi} \right), \, \gamma = \frac{\sin a\pi}{a\pi}.$$

Lemma B.2. Let A be an arbitrary linear operator, G be a Hermitian unitary and $V = e^{-i\frac{\theta}{2}G}$. Let O be an arbitrary Hermitian operator that anti-commutes with G, and \tilde{O} be an arbitrary Hermitian operator that commutes with G. Then,

$$\mathbb{E} \operatorname{Tr} \left[OVAV^{\dagger} \right] = \gamma \operatorname{Tr} \left[OA \right], \tag{B1}$$

$$\mathbb{E}_{a} \frac{\partial}{\partial \theta} \operatorname{Tr} \left[OVAV^{\dagger} \right] = \gamma \operatorname{Tr} \left[iGOA \right], \tag{B2}$$

$$\mathbb{E}_{\theta} \operatorname{Tr} \left[\tilde{O} V A V^{\dagger} \right] = \operatorname{Tr} \left[\tilde{O} A \right], \tag{B3}$$

$$\mathbb{E}_{\theta} \frac{\partial}{\partial \theta} \operatorname{Tr} \left[\tilde{O} V A V^{\dagger} \right] = 0. \tag{B4}$$

Proof. From $V=e^{-i\frac{\theta}{2}G}=I\cos\frac{\theta}{2}-iG\sin\frac{\theta}{2},$ for any operator B, we have

$$\operatorname{Tr}\left[BVAV^{\dagger}\right]$$

$$=\operatorname{Tr}\left[B(I\cos\frac{\theta}{2}-iG\sin\frac{\theta}{2})A(I\cos\frac{\theta}{2}+iG\sin\frac{\theta}{2})\right]$$

$$=\frac{1+\cos\theta}{2}\operatorname{Tr}\left[BA\right]+\frac{1-\cos\theta}{2}\operatorname{Tr}\left[BGAG\right]$$

$$+\frac{\sin\theta}{2}\left(\operatorname{Tr}\left[iBAG\right]-\operatorname{Tr}\left[iBGA\right]\right). \tag{B5}$$

If O anti-commutes with G, then iGO is Hermitian. In addition, with G being unitary and $\{O,G\}=0$, from Eq. (B5) we have

$$\operatorname{Tr}\left[OVAV^{\dagger}\right] = \cos\theta \operatorname{Tr}\left[OA\right] + \sin\theta \operatorname{Tr}\left[iGOA\right], \quad (B6)$$

and accordingly,

$$\frac{\partial}{\partial \theta} \operatorname{Tr} \left[OVAV^{\dagger} \right] = -\sin \theta \operatorname{Tr} \left[OA \right] + \cos \theta \operatorname{Tr} \left[iGOA \right]. \tag{B7}$$

Thus, Eqs. (B1) and (B2) can be obtained by taking the expectations of Eqs. (B6) and (B7) over θ , respectively.

Moreover, when \tilde{O} commutes with the unitary G, following similar calculations, it is straightforward to have Eqs. (B3) and (B4).

From Lemma B.2, we have the following conclusion.

Corollary B.3. Let A be an arbitrary linear operator, G be a Hermitian unitary and $V = e^{-i\frac{\theta}{2}G}$. Let O denote an arbitrary Hermitian operator that anti-commutes with G, and \tilde{O}_1 and \tilde{O}_2 be arbitrary Hermitian operators that commute with G. Then,

$$\mathbb{E}_{\theta} \operatorname{Tr} \left[OVAV^{\dagger} \right] \operatorname{Tr} \left[\tilde{O}_{1}VAV^{\dagger} \right] = \gamma \operatorname{Tr} \left[OA \right] \operatorname{Tr} \left[\tilde{O}_{1}A \right],$$
(B8)

$$\mathbb{E}_{\theta} \frac{\partial}{\partial \theta} \operatorname{Tr} \left[OVAV^{\dagger} \right] \frac{\partial}{\partial \theta} \operatorname{Tr} \left[\tilde{O}_{1} VAV^{\dagger} \right] = 0, \tag{B9}$$

$$\mathbb{E}_{\theta} \operatorname{Tr} \left[\tilde{O}_{1} V A V^{\dagger} \right] \operatorname{Tr} \left[\tilde{O}_{2} V A V^{\dagger} \right] = \operatorname{Tr} \left[\tilde{O}_{1} A \right] \operatorname{Tr} \left[\tilde{O}_{2} A \right],$$
(B10)

$$\mathbb{E}_{\theta} \frac{\partial}{\partial \theta} \operatorname{Tr} \left[\tilde{O}_1 V A V^{\dagger} \right] \frac{\partial}{\partial \theta} \operatorname{Tr} \left[\tilde{O}_2 V A V^{\dagger} \right] = 0. \tag{B11}$$

Lemma B.4. Let A be an arbitrary linear operator, G be a Hermitian unitary and $V = e^{-i\frac{\theta}{2}G}$. Let O_1 and O_2 be arbitrary Hermitian operators that anti-commute with G. Then,

$$\mathbb{E} \operatorname{Tr} \left[O_{1}VAV^{\dagger} \right] \operatorname{Tr} \left[O_{2}VAV^{\dagger} \right]$$

$$= \alpha \operatorname{Tr} \left[O_{1}A \right] \operatorname{Tr} \left[O_{2}A \right] + \beta \operatorname{Tr} \left[iGO_{1}A \right] \operatorname{Tr} \left[iGO_{2}A \right], (B12)$$

$$\mathbb{E} \frac{\partial}{\partial \theta} \operatorname{Tr} \left[O_{1}VAV^{\dagger} \right] \frac{\partial}{\partial \theta} \operatorname{Tr} \left[O_{2}VAV^{\dagger} \right]$$

$$= \beta \operatorname{Tr} \left[O_{1}A \right] \operatorname{Tr} \left[O_{2}A \right] + \alpha \operatorname{Tr} \left[iGO_{1}A \right] \operatorname{Tr} \left[iGO_{2}A \right]. (B13)$$

Proof. According to Eqs. (B6) and B7), we have

$$\operatorname{Tr}\left[O_{1}VAV^{\dagger}\right]\operatorname{Tr}\left[O_{2}VAV^{\dagger}\right]$$

$$= \cos^{2}\theta\operatorname{Tr}\left[O_{1}A\right]\operatorname{Tr}\left[O_{2}A\right] + \sin^{2}\theta\operatorname{Tr}\left[iGO_{1}A\right]\operatorname{Tr}\left[iGO_{2}A\right]$$

$$+ \sin\theta\cos\theta\left(\operatorname{Tr}\left[O_{1}A\right]\operatorname{Tr}\left[iGO_{2}A\right]\right)$$

$$+ \operatorname{Tr}\left[O_{2}A\right]\operatorname{Tr}\left[iGO_{1}A\right]\right), \qquad (B14)$$

$$\frac{\partial}{\partial\theta}\operatorname{Tr}\left[O_{1}VAV^{\dagger}\right]\frac{\partial}{\partial\theta}\operatorname{Tr}\left[O_{2}VAV^{\dagger}\right]$$

$$= \sin^{2}\theta\operatorname{Tr}\left[O_{1}A\right]\operatorname{Tr}\left[O_{2}A\right] + \cos^{2}\theta\operatorname{Tr}\left[iGO_{1}A\right]\operatorname{Tr}\left[iGO_{2}A\right]$$

$$- \sin\theta\cos\theta\left(\operatorname{Tr}\left[O_{1}A\right]\operatorname{Tr}\left[iGO_{2}A\right]\right]$$

Then, Eqs. (B12) and (B13) can be derived by taking the expectations of Eqs. (B14) and (B15) and employing

 $+\operatorname{Tr}\left[O_{2}A\right]\operatorname{Tr}\left[iGO_{1}A\right]$.

$$\mathbb{E}_{\theta} \cos^2 \theta = \alpha, \ \mathbb{E}_{\theta} \sin^2 \theta = \beta, \ \mathbb{E}_{\theta} \sin \theta \cos \theta = 0.$$

It follows that the following conclusion holds.

(B15)

Corollary B.5. Let A be an arbitrary linear operator, G be a Hermitian unitary and $V = e^{-i\frac{\theta}{2}G}$. Let O be an arbitrary Hermitian operator that anti-commutes with G. Then,

$$\mathbb{E} \operatorname{Tr}^{2} \left[OVAV^{\dagger} \right] = \alpha \operatorname{Tr}^{2} \left[OA \right] + \beta \operatorname{Tr}^{2} \left[iGOA \right], \quad (B16)$$

$$\mathbb{E} \left(\frac{\partial}{\partial \theta} \operatorname{Tr} \left[OVAV^{\dagger} \right] \right)^{2} = \beta \operatorname{Tr}^{2} \left[OA \right] + \alpha \operatorname{Tr}^{2} \left[iGOA \right], \quad (B17)$$

where $\operatorname{Tr}^2[\cdot] = (\operatorname{Tr}[\cdot])^2$.

The following lemma concerns the transformations of 2-qubit Pauli tensor products after a controlled-Z gate.

Lemma B.6. Let CZ denote a controlled-Z gate, and $\sigma_i \otimes \sigma_j$ be a 2-qubit Pauli tensor product, where σ_i and σ_j are Pauli matrices. If $\sigma_{i'} \otimes \sigma_{j'} = CZ^{\dagger}(\sigma_i \otimes \sigma_j)CZ$, we denote the transformation by $\sigma_i \otimes \sigma_j \to \sigma_{i'} \otimes \sigma_{j'}$. All of the specific transformations can be summarized as follows:

$$Z \otimes I \leftrightarrow Z \otimes I, \quad Z \otimes Z \leftrightarrow Z \otimes Z,$$
$$Y \otimes I \leftrightarrow Y \otimes Z, \quad Y \otimes Y \leftrightarrow X \otimes X,$$
$$X \otimes I \leftrightarrow X \otimes Z, \quad X \otimes Y \leftrightarrow -Y \otimes X.$$

Appendix C: Proof of Theorem III.1

Proof. For the warm-up Hamiltonian of Eq. (4), the average of the squared norm of the gradient can be described

$$\mathbb{E} \|\nabla_{\boldsymbol{\theta}} C\|_{2}^{2} = \sum_{q=1}^{2L} \sum_{n=1}^{N} \mathbb{E} \left(\frac{\partial C}{\partial \theta_{q,n}} \right)^{2}$$

$$= \sum_{q=1}^{2L} \sum_{n=1}^{N} \mathbb{E} \left(\sum_{i=1}^{N-1} \frac{\partial C_{i}}{\partial \theta_{q,n}} \right)^{2}$$

$$= \sum_{i=1}^{N-1} \sum_{q=1}^{2L} \sum_{n=1}^{N} \mathbb{E} \left(\frac{\partial C_{i}}{\partial \theta_{q,n}} \right)^{2}$$

$$+ \sum_{i \neq i-1}^{N-1} \sum_{q=1}^{2L} \sum_{n=1}^{N} \mathbb{E} \left(\frac{\partial C_{i}}{\partial \theta_{q,n}} \frac{\partial C_{j}}{\partial \theta_{q,n}} \right), (C1)$$

where $C_i = \text{Tr} \left[Z_i Z_{i+1} U(\boldsymbol{\theta}) \rho U^{\dagger}(\boldsymbol{\theta}) \right]$. Thus, we turn to analyze the lower bound of Eq. (C1).

For clarity, we first introduce notation. As illustrated in Fig. 1(a), the *L*-layer parameterized unitary $U(\theta)$ can be expressed as the product of *L* sequential unitaries

$$U(\boldsymbol{\theta}) = U_L(\boldsymbol{\theta}_{2L}, \boldsymbol{\theta}_{2L-1}) \cdots U_1(\boldsymbol{\theta}_2, \boldsymbol{\theta}_1),$$

with

$$U_{l}(\boldsymbol{\theta}_{2l}, \boldsymbol{\theta}_{2l-1}) = R_{2l}(\boldsymbol{\theta}_{2l}) R_{2l-1}(\boldsymbol{\theta}_{2l-1}) CZ_{l},$$

$$R_{2l}(\boldsymbol{\theta}_{2l}) = e^{-\frac{i}{2}\theta_{2l,1}Y} \otimes \cdots \otimes e^{-\frac{i}{2}\theta_{2l,N}Y},$$

$$R_{2l-1}(\boldsymbol{\theta}_{2l-1}) = e^{-\frac{i}{2}\theta_{2l-1,1}X} \otimes \cdots \otimes e^{-\frac{i}{2}\theta_{2l-1,N}X}.$$

Here, for $l \in [L]$, CZ_l denotes the lth entanglement layer composed of arbitrarily many CZ gates, and $R_{2l}(\boldsymbol{\theta}_{2l})$ and $R_{2l-1}(\boldsymbol{\theta}_{2l-1})$ denote the lth R_Y and R_X rotation layer, respectively. Denote $\rho_0 = |0\rangle \langle 0|$, and for $l \in [L]$, let

$$\begin{cases} \rho_{2l} = R_{2l}(\boldsymbol{\theta}_{2l})\rho_{2l-1}R_{2l}^{\dagger}(\boldsymbol{\theta}_{2l}), \\ \rho_{2l-1} = R_{2l-1}(\boldsymbol{\theta}_{2l-1})CZ_{l}\rho_{2l-2}CZ_{l}^{\dagger}R_{2l-1}^{\dagger}(\boldsymbol{\theta}_{2l-1}). \end{cases}$$

Now we evaluate the lower bound of the first summation in Eq. (C1). Note that

$$\mathbb{E}\left(\frac{\partial C_{i}}{\partial \theta_{q,n}}\right)^{2}$$

$$= \mathbb{E}\left(\frac{\partial}{\partial \theta_{q,n}} \operatorname{Tr}\left[Z_{i}Z_{i+1}U(\theta)\rho_{0}U^{\dagger}(\theta)\right]\right)^{2}$$

$$= \mathbb{E}\left(\frac{\partial}{\partial \theta_{q,n}} \operatorname{Tr}\left[Z_{i}Z_{i+1}\rho_{2L}\right]\right)^{2}$$

$$= \mathbb{E}\left(\frac{\partial}{\partial \theta_{q,n}} \operatorname{Tr}\left[Z_{i}Z_{i+1}R_{2L}(\theta_{2L})\rho_{2L-1}R_{2L}^{\dagger}(\theta_{2L})\right]\right)^{2} (C2a)$$

$$= \mathbb{E}\left[\mathbb{$$

Here, Eq. (C2b) is due to the linearity of the trace operation, which is frequently utilized in the proof. Eq. (C2c) is obtained by first employing Eq. (B16) to take the expectations over $\theta_{2L,i}$ and $\theta_{2L,i+1}$ producing the coefficient α^2 , and then leveraging Eq. (B10) to take the expectations over the other N-2 components in θ_{2L} . Following a similar analysis, Eq. (C2d) can be derived. Eq. (C2e) is due to Lemma B.6, that is, the tensor product $Z_i Z_{i+1}$ remains unchanged after applying arbitrarily many CZ gates.

We repeat the techniques for deriving Eqs. (C2a)-(C2e) to calculate the expectations over $\theta_{2L-1}, \ldots, \theta_{q+1}$ and obtain

$$\mathbb{E}\left(\frac{\partial C_i}{\partial \theta_{q,n}}\right)^2 \ge \alpha^{2(2L-q)} \mathbb{E}_{\boldsymbol{\theta}_{[q]}} \left(\frac{\partial}{\partial \theta_{q,n}} \operatorname{Tr}\left[Z_i Z_{i+1} \rho_q\right]\right)^2. \tag{C3}$$

Next, we proceed upon the index n, the ordinal number of the qubit where the trainable parameter $\theta_{q,n}$ lies. In the case where $n \in \{i, i+1\}$, we have

$$\mathbb{E}\left(\frac{\partial C_{i}}{\partial \theta_{q,n}}\right)^{2} \geq \alpha^{2(2L-q)} \alpha \beta \mathbb{E}_{\theta_{[q-1]}} \operatorname{Tr}^{2} \left[Z_{i} Z_{i+1} \rho_{q-1}\right]$$
(C4a)
$$\geq \alpha^{2(2L-q)+1} \beta \alpha^{2(q-1)} \operatorname{Tr}^{2} \left[Z_{i} Z_{i+1} \rho_{0}\right],$$
(C4b)

where β in Eq. (C4a) is obtained by employing Eq. (B17) to take the expectation over $\theta_{q,n}$. It is worth pointing out that to persist the observable $Z_i Z_{i+1}$ in the following analysis, we keep the item with coefficient β rather than α in the inequality. As for the other N-1 components in θ_q , the analysis is the same as that in Eq. (C2c) or (C2d). Following a similar derivation to Eq. (C3), Eq. (C4b) can be obtained.

In the case where $n \notin \{i, i+1\}$, when taking the expectation over $\theta_{q,n}$, by Eq. (B11) we have

$$\underset{\boldsymbol{\theta}_{[q]}}{\mathbb{E}} \left(\frac{\partial}{\partial \theta_{q,n}} \operatorname{Tr} \left[Z_i Z_{i+1} \rho_q \right] \right)^2 = 0. \tag{C5}$$

Therefore, combining Eq. (C4b) and Eq. (C5), it can be seen that

$$\mathbb{E}\left(\frac{\partial C_i}{\partial \theta_{q,n}}\right)^2 \ge \begin{cases} \alpha^{4L-1}\beta, & n \in \{i, i+1\}, \\ 0, & \text{otherwise,} \end{cases}$$
(C6)

and the first summation in Eq. (C1) is lower bounded by

$$\sum_{i=1}^{N-1} \sum_{q=1}^{2L} \sum_{n=1}^{N} \mathbb{E} \left(\frac{\partial C_i}{\partial \theta_{q,n}} \right)^2 \ge (N-1) \times 2L \times 2\alpha^{4L-1}\beta. \tag{C7}$$

Then, we analyze the second summation in Eq. (C1). Note that

$$\mathbb{E}\left(\frac{\partial C_{i}}{\partial \theta_{q,n}} \frac{\partial C_{j}}{\partial \theta_{q,n}}\right)$$

$$= \mathbb{E}\left(\frac{\partial}{\partial \theta_{q,n}} \operatorname{Tr}\left[Z_{i} Z_{i+1} \rho_{2L}\right] \frac{\partial}{\partial \theta_{q,n}} \operatorname{Tr}\left[Z_{j} Z_{j+1} \rho_{2L}\right]\right).$$

We first consider the case where $\{i, i+1\} \cap \{j, j+1\} = \emptyset$.

$$\mathbb{E}\left(\frac{\partial C_{i}}{\partial \theta_{q,n}} \frac{\partial C_{j}}{\partial \theta_{q,n}}\right)$$

$$= \gamma^{4(2L-q)} \mathbb{E}_{\theta_{[q]}} \left(\frac{\partial}{\partial \theta_{q,n}} \operatorname{Tr}\left[Z_{i}Z_{i+1}\rho_{q}\right] \frac{\partial}{\partial \theta_{q,n}} \operatorname{Tr}\left[Z_{j}Z_{j+1}\rho_{q}\right]\right)$$
(C8a)

$$=0. (C8b)$$

In regard to the expectation over θ_{2L} in Eq. (C8a), the coefficient γ appears each time when we take the expectation over $\theta_{2L,i}$, $\theta_{2L,i+1}$, $\theta_{2L,j}$ or $\theta_{2L,j+1}$ by employing Eq. (B8). In addition, Eq. (B10) is utilized to calculate

the expectations over the other components in $\boldsymbol{\theta}_{2L}$. Similarly, we can take the expectations over $\boldsymbol{\theta}_{2L-1},\ldots,\boldsymbol{\theta}_{q+1}$, during which the calculation of each CZ_l layer is the same as that in Eq. (C2e). When taking the expectation over $\boldsymbol{\theta}_{q,n}$, Eq. (C8b) can be obtained by employing either Eq. (B9) for $n \in \{i, i+1, j, j+1\}$ or Eq. (B11), otherwise.

Next, we consider the case where i = j + 1 or i + 1 = j. Let us consider the case i + 1 = j in detail, and the other case can be followed in a similar way. Note that

$$\mathbb{E}\left(\frac{\partial C_{i}}{\partial \theta_{q,n}} \frac{\partial C_{i+1}}{\partial \theta_{q,n}}\right) \\
= \mathbb{E}\left(\frac{\partial}{\partial \theta_{q,n}} \operatorname{Tr}\left[Z_{i}Z_{i+1}\rho_{2L}\right] \frac{\partial}{\partial \theta_{q,n}} \operatorname{Tr}\left[Z_{i+1}Z_{i+2}\rho_{2L}\right]\right) \\
= \gamma^{2} \alpha \mathbb{E}\left(\frac{\partial}{\partial \theta_{q,n}} \operatorname{Tr}\left[Z_{i}Z_{i+1}\rho_{2L-1}\right] \right) \\
= \frac{\partial}{\partial \theta_{q,n}} \operatorname{Tr}\left[Z_{i}Z_{i+1}\rho_{2L-1}\right] \\
+ \gamma^{2} \beta \mathbb{E}\left(\frac{\partial}{\partial \theta_{q,n}} \operatorname{Tr}\left[Z_{i}X_{i+1}\rho_{2L-1}\right]\right) \\
= \gamma^{4} \alpha^{2} \mathbb{E}\left(\frac{\partial}{\partial \theta_{q,n}} \operatorname{Tr}\left[Z_{i}X_{i+1}\rho_{2L-1}\right]\right) \\
= \frac{\partial}{\partial \theta_{q,n}} \operatorname{Tr}\left[\operatorname{CZ}_{L}^{\dagger}Z_{i}Z_{i+1}\operatorname{CZ}_{L}\rho_{2L-2}\right] \\
\frac{\partial}{\partial \theta_{q,n}} \operatorname{Tr}\left[\operatorname{CZ}_{L}^{\dagger}Z_{i+1}Z_{i+2}\operatorname{CZ}_{L}\rho_{2L-2}\right] \\
+ \gamma^{4} \alpha \beta \mathbb{E}\left(\frac{\partial}{\partial \theta_{q,n}} \operatorname{Tr}\left[\operatorname{CZ}_{L}^{\dagger}Z_{i}Y_{i+1}\operatorname{CZ}_{L}\rho_{2L-2}\right] \\
\frac{\partial}{\partial \theta_{q,n}} \operatorname{Tr}\left[\operatorname{CZ}_{L}^{\dagger}Z_{i}X_{i+1}\operatorname{CZ}_{L}\rho_{2L-2}\right] \\
+ \gamma^{4} \beta \mathbb{E}\left(\frac{\partial}{\partial \theta_{q,n}} \operatorname{Tr}\left[\operatorname{CZ}_{L}^{\dagger}Z_{i}X_{i+1}\operatorname{CZ}_{L}\rho_{2L-2}\right] \\
\frac{\partial}{\partial \theta_{q,n}} \operatorname{Tr}\left[\operatorname{CZ}_{L}^{\dagger}Z_{i}X_{i+1}\operatorname{CZ}_$$

Here, Eq. (C9b) is obtained by taking the expectations over $\theta_{2L,i+1}$ by Eq. (B12), $\theta_{2L,i}$ and $\theta_{2L,i+2}$ by Eq. (B8), and the other N-3 components by Eq. (B10). Similarly, Eq. (C9c) can be derived.

It is worth pointing out that after employing Lemmas B.2 and B.4 to calculate the expectations over the trainable parameters in rotation layers, except for the terms related to the original observables Z_iZ_{i+1} and $Z_{i+1}Z_{i+2}$, other terms related to new observables may be generated. For example, after taking the expectation over θ_{2L} , the original observable Z_iZ_{i+1} in Eq. (C9a) generates two terms related to the observable Z_iZ_{i+1} and Z_iX_{i+1} , respectively, in Eq. (C9b). It is clear that the generated new observables are always N-qubit Pauli

strings as defined in Eq. (1), and the corresponding coefficients are monomials of γ , α and β , which are always positive. Moreover, according to Lemma B.6, after applying an entanglement layer composed of CZ gates, the generated observables are still N-qubit Pauli strings, where, for example, the observable Z_iZ_{i+1} remains unchanged. Thus, whenever we finish the calculations with respect to a block, there are always terms related to the original observables Z_iZ_{i+1} and $Z_{i+1}Z_{i+2}$, and some other generated terms related to observables in the form of N-qubit Pauli strings. We point out that all the generated terms are non-negative, and we come back to its proof later. In the following, the terms with the original observables Z_iZ_{i+1} and $Z_{i+1}Z_{i+2}$ are kept only for further analysis. Thus, we have

$$\mathbb{E}\left(\frac{\partial C_{i}}{\partial \theta_{q,n}} \frac{\partial C_{i+1}}{\partial \theta_{q,n}}\right)$$

$$\geq \gamma^{4} \alpha^{2} \mathbb{E}_{\theta_{[2L-2]}} \left(\frac{\partial}{\partial \theta_{q,n}} \operatorname{Tr}\left[Z_{i} Z_{i+1} \rho_{2L-2}\right]\right)$$

$$\frac{\partial}{\partial \theta_{q,n}} \operatorname{Tr}\left[Z_{i+1} Z_{i+2} \rho_{2L-2}\right]\right) \qquad (C10a)$$

$$\geq \gamma^{2(2L-q)} \alpha^{2L-q} \mathbb{E}_{\theta_{[q]}} \left(\frac{\partial}{\partial \theta_{q,n}} \operatorname{Tr}\left[Z_{i} Z_{i+1} \rho_{q}\right]\right)$$

$$\frac{\partial}{\partial \theta_{q,n}} \operatorname{Tr}\left[Z_{i+1} Z_{i+2} \rho_{q}\right]$$

$$\frac{\partial}{\partial \theta_{q,n}} \operatorname{Tr}\left[Z_{i+1} Z_{i+2} \rho_{q}\right]$$

$$(C10b)$$

where Eq. (C10b) is obtained by repeating the same analysis as that in Eq. (C10a) for the expectations over $\theta_{2L-2}, \ldots, \theta_{q+1}$.

Then, we proceed upon the index n. When n = i + 1, we have

$$\mathbb{E}_{\boldsymbol{\theta}_{[q]}} \left(\frac{\partial}{\partial \theta_{q,n}} \operatorname{Tr} \left[Z_i Z_{i+1} \rho_q \right] \frac{\partial}{\partial \theta_{q,n}} \operatorname{Tr} \left[Z_{i+1} Z_{i+2} \rho_q \right] \right)
\geq \gamma^2 \beta \mathbb{E}_{\boldsymbol{\theta}_{[q-1]}} \left(\operatorname{Tr} \left[Z_i Z_{i+1} \rho_{q-1} \right] \operatorname{Tr} \left[Z_{i+1} Z_{i+2} \rho_{q-1} \right] \right) \quad (C11a)
\geq \gamma^2 \beta \gamma^{2(q-1)} \alpha^{q-1} \operatorname{Tr} \left[Z_i Z_{i+1} \rho_0 \right] \operatorname{Tr} \left[Z_{i+1} Z_{i+2} \rho_0 \right], \quad (C11b)$$

where in Eq. (C11a), the coefficient β comes from Eq. (B13) for the expectation over $\theta_{q,n}$, and the coefficient γ^2 comes from Eq. (B8) for $\theta_{q,n-1}$ and $\theta_{q,n+1}$. Eq. (C11b) is obtained in the same way as Eq. (C10b).

When $n \neq i+1$, by employing either Eq. (B9) for $n \in \{i, i+2\}$ or Eq. (B11), otherwise, to take the expectation over $\theta_{q,n}$, we have

$$\underset{\boldsymbol{\theta}_{[q]}}{\mathbb{E}} \left(\frac{\partial}{\partial \theta_{q,n}} \operatorname{Tr} \left[Z_i Z_{i+1} \rho_q \right] \frac{\partial}{\partial \theta_{q,n}} \operatorname{Tr} \left[Z_{i+1} Z_{i+2} \rho_q \right] \right) = 0.$$
(C12)

Now we prove the non-negativity of the generated terms. Without loss of generality, we take the inequality in Eq. (C11b) as an example. The gap between the interested term (C9a) and the final term (C11b) can be expressed exactly as a linear combination of all generated

terms

$$\sum_{k} c_{k} \operatorname{Tr} \left[\boldsymbol{\sigma}_{\boldsymbol{g}_{i}^{k}} \rho_{0} \right] \operatorname{Tr} \left[\boldsymbol{\sigma}_{\boldsymbol{g}_{i+1}^{k}} \rho_{0} \right], \quad (C13)$$

where c_k is the positive coefficient, $\sigma_{g_i^k}$ and $\sigma_{g_{i+1}^k}$ denote the N-qubit Pauli strings generated from $Z_i Z_{i+1}$ and $Z_{i+1} Z_{i+2}$, but not themselves, respectively. With the choice of the initial state $\rho_0 = |0\rangle \langle 0|$, other terms like Eq. (C13) are always non-negative.

Therefore, from Eqs. (C10b), (C11b), and (C12), we have

$$\mathbb{E}\left(\frac{\partial C_i}{\partial \theta_{q,n}} \frac{\partial C_j}{\partial \theta_{q,n}}\right) \ge \begin{cases} \gamma^{4L} \alpha^{2L-1} \beta, & n = i = j+1, \\ \gamma^{4L} \alpha^{2L-1} \beta, & n = i+1 = j, \\ 0, & \text{otherwise,} \end{cases}$$

and the second summation in Eq. (C1) is lower bounded by

$$\sum_{i \neq j=1}^{N-1} \sum_{q=1}^{2L} \sum_{n=1}^{N} \mathbb{E}\left(\frac{\partial C_i}{\partial \theta_{q,n}} \frac{\partial C_j}{\partial \theta_{q,n}}\right) \ge 2(N-2) \times 2L\gamma^{4L} \alpha^{2L-1} \beta. \tag{C14}$$

Combining Eq. (C7) and Eq. (C14), we have $\mathbb{E} \|\nabla_{\boldsymbol{\theta}} C\|_{2}^{2} \geq 4(N-1)L\alpha^{4L-1}\beta + 4(N-2)L\gamma^{4L}\alpha^{2L-1}\beta$ $\geq 4(2N-3)L\gamma^{8L-2}\beta, \qquad (C15)$

where the second inequality is derived by using the inequality

$$\alpha = \frac{1}{4} \left(2 + \frac{\sin 2a\pi}{a\pi} \right) \ge \gamma^2 = \left(\frac{\sin a\pi}{a\pi} \right)^2, \ a \in (0, 1).$$

Finally, we determine the hyperparameter a. Let x denote $(a\pi)^2$. It can be verified that for $a \in (0,1)$,

$$\begin{split} \gamma & \geq 1 - \tfrac{1}{6}a^2\pi^2 = 1 - \tfrac{1}{6}x, \\ \beta & \geq \tfrac{1}{3}a^2\pi^2 - \tfrac{1}{15}a^4\pi^4 = \tfrac{1}{3}x - \tfrac{1}{15}x^2. \end{split}$$

In order to ensure the positivity of the right sides of the two inequalities above, we further set $a \in \left(0, \frac{\sqrt{5}}{\pi}\right)$, i.e., $x \in (0,5)$. Then, the lower bound in Eq. (5), that is, Eq. (C15) can be further bounded by

$$4(2N-3)L\left(\frac{1}{3}x-\frac{1}{15}x^2\right)\left(1-\frac{1}{6}x\right)^{8L-2} \triangleq g(N,L,x).$$

It can be verified that g(N, L, x) attains its maximum when

$$x = \frac{40L + 7 - \sqrt{1600L^2 - 400L + 49}}{16L}.$$

Thus, we choose the hyperparameter as

$$a = \frac{1}{4\pi} \sqrt{\frac{40L + 7 - \sqrt{1600L^2 - 400L + 49}}{L}}, \quad (C16)$$

which has the same scaling as $\frac{1}{\sqrt{L}}$, that is, $a \in \Theta\left(\frac{1}{\sqrt{L}}\right)$. Moreover, with the selected a in Eq. (C16), g(N, L, a) can be lower bounded by

$$g(N, L, a) \ge e^{-1}(2N - 3),$$

which is obtained by the fact that the function $\frac{1}{2N-3}g(N,L,a)$ decreases monotonically with L and converges to e^{-1} .

Appendix D: Proof of Theorem III.2

We continue to utilize the notation in Appendix C. In addition, for each term σ_i in Eq. (3), denote S^i as the number of nonzero components in the vector $i = (i_1, i_2, \dots, i_N)$. According to the definition of S-local cost function in the form of Eq. (3), we have $S^i \leq S$. The number of elements being j in vector i is denoted by S^i_j , for $j \in \{1, 2, 3\}$. Thus, we have

$$S^{i} = S_1^{i} + S_2^{i} + S_3^{i} \le S. \tag{D1}$$

We introduce $I_{S^i} \triangleq \{n \mid i_n \neq 0, n \in [N]\}$ to denote the set of qubits upon which the term σ_i acts non-trivially. Similarly, we define $I_{S^i_j} \triangleq \{n | i_n = j, n \in [N]\}$ for $j \in \{1, 2, 3\}$.

Moreover, for $i = (i_1, i_2, \dots, i_N)$, $i_j \in \{0, 1, 2, 3\}$, $j \in [N]$, let $\mathbf{3} : i$ denote the N-dimensional vector after replacing all nonzero components in i with 3, and $\mathbf{3} : i; \mathbf{1}$ denote the N-dimensional vector after replacing all 1s in i with 3.

Proof. For the general Hamiltonian of Eq. (3), the expectation of the squared norm of the gradient of the cost function can be described as

$$\mathbb{E} \|\nabla_{\boldsymbol{\theta}} C\|_{2}^{2} = \sum_{q=1}^{2L} \sum_{n=1}^{N} \mathbb{E} \left(\frac{\partial C}{\partial \theta_{q,n}} \right)^{2}$$

$$= \sum_{q=1}^{2L} \sum_{n=1}^{N} \mathbb{E} \left(\sum_{i \in \mathcal{N}} \frac{\partial C_{i}}{\partial \theta_{q,n}} \right)^{2}$$

$$= \sum_{i \in \mathcal{N}} \sum_{q=1}^{2L} \sum_{n=1}^{N} \mathbb{E} \left(\frac{\partial C_{i}}{\partial \theta_{q,n}} \right)^{2}$$

$$+ \sum_{i \neq j \in \mathcal{N}} \sum_{q=1}^{2L} \sum_{n=1}^{N} \mathbb{E} \left(\frac{\partial C_{i}}{\partial \theta_{q,n}} \right)^{2}$$

$$+ \sum_{i \neq j \in \mathcal{N}} \sum_{q=1}^{2L} \sum_{n=1}^{N} \mathbb{E} \left(\frac{\partial C_{i}}{\partial \theta_{q,n}} \frac{\partial C_{j}}{\partial \theta_{q,n}} \right), (D2)$$

where $C_i = \text{Tr} \left[\boldsymbol{\sigma}_i U(\boldsymbol{\theta}) \rho U^{\dagger}(\boldsymbol{\theta}) \right]$. Thus, we turn to analyze the lower bound of Eq. (D2).

For the first summation in Eq. (D2), we have

$$\sum_{\boldsymbol{i} \in \mathcal{N}} \sum_{q=1}^{2L} \sum_{n=1}^{N} \mathbb{E}_{\boldsymbol{\theta}} \left(\frac{\partial C_{\boldsymbol{i}}}{\partial \theta_{q,n}} \right)^2 \geq \sum_{\boldsymbol{i} \in \mathcal{N}} \sum_{q=1}^{2L-2} \sum_{n=1}^{N} \mathbb{E}_{\boldsymbol{\theta}} \left(\frac{\partial C_{\boldsymbol{i}}}{\partial \theta_{q,n}} \right)^2.$$

Note that, for $q \in [2L - 2]$,

$$\mathbb{E}\left(\frac{\partial C_{i}}{\partial \theta_{q,n}}\right)^{2}$$

$$= \mathbb{E}\left(\frac{\partial}{\partial \theta_{q,n}} \operatorname{Tr}\left[\boldsymbol{\sigma}_{i}\rho_{2L}\right]\right)^{2}$$

$$= \mathbb{E}\left(\frac{\partial}{\partial \theta_{q,n}} \operatorname{Tr}\left[\boldsymbol{\sigma}_{i}\rho_{2L}\right]\right)^{2}$$

$$= \mathbb{E}\mathbb{E}\left[\mathbb{E}\left(\frac{\partial}{\partial \theta_{q,n}} \operatorname{Tr}\left[\boldsymbol{\sigma}_{i}R_{2L}(\boldsymbol{\theta}_{2L})\rho_{2L-1}R_{2L}^{\dagger}(\boldsymbol{\theta}_{2L})\right]\right)^{2}$$

$$\geq \alpha^{S_{3}^{i}}\beta^{S_{1}^{i}}\mathbb{E}\left(\frac{\partial}{\partial \theta_{q,n}} \operatorname{Tr}\left[\boldsymbol{\sigma}_{3:i;1}\rho_{2L-1}\right]\right)^{2} \qquad (D3a)$$

$$\geq \alpha^{S_{1}^{i}+2S_{3}^{i}}\beta^{S_{1}^{i}+S_{2}^{i}}$$

$$\mathbb{E}\left(\frac{\partial}{\partial \theta_{q,n}} \operatorname{Tr}\left[\operatorname{CZ}_{L}^{\dagger}\boldsymbol{\sigma}_{3:i}\operatorname{CZ}_{L}\rho_{2L-2}\right]\right)^{2} (D3b)$$

$$= \alpha^{S_{1}^{i}+2S_{3}^{i}}\beta^{S_{1}^{i}+S_{2}^{i}}\mathbb{E}\left(\frac{\partial}{\partial \theta_{q,n}} \operatorname{Tr}\left[\boldsymbol{\sigma}_{3:i}\rho_{2L-2}\right]\right)^{2}, (D3c)$$

where Eq. (D3a) is obtained by using Eq. (B16) up to $S_3^i + S_1^i$ times with respect to $\theta_{2L,n}, n \in I_{S_3^i} \cup I_{S_1^i}$, and using Eq. (B10) up to $N - S_3^i - S_1^i$ times with respect to the other components in θ_{2L} . The appearance of the coefficient $\alpha^{S_3^i}\beta^{S_1^i}$ is due to the fact that each time when Eq. (B16) is employed we only keep the item with more Pauli Z tensors in the corresponding N-qubit Pauli string observable. Eq. (D3b) is derived by using Eq. (B16) up to S^i times with respect to $\theta_{2L-1,n}, n \in I_{S^i}$ with the appearance of the coefficient $\alpha^{S_1^i+S_3^i}\beta^{S_2^i}$, and using Eq. (B10) up to $N-S^i$ times with respect to the remain components in θ_{2L-1} . Eq. (D3c) follows the same reasoning behind Eq. (C2e).

After taking the expectations over θ_{2L} and θ_{2L-1} , the observable remained in Eq. (D3c) is $\sigma_{3:i}$, which is an N-qubit tensor product composed of identity and at most S Pauli Z operators. Thus, to bound the expectation term in Eq. (D3c), we can employ the same technique used for the interested term (C6) related to the original observable $Z_i Z_{i+1}$, specifically,

$$\underset{\boldsymbol{\theta}_{[2L-2]}}{\mathbb{E}} \left(\frac{\partial}{\partial \boldsymbol{\theta}_{q,n}} \mathrm{Tr} \left[\boldsymbol{\sigma_{3:i}} \rho_{2L-2} \right] \right)^2 \geq \begin{cases} \alpha^{2S^i(L-1)-1} \beta, n \in I_{S^i}, \\ 0, & \text{otherwise.} \end{cases}$$

Thus, the first summation in Eq. (D2) is lower bounded by

$$\sum_{i \in \mathcal{N}} \sum_{q=1}^{2L} \sum_{n=1}^{N} \mathbb{E} \left(\frac{\partial C_{i}}{\partial \theta_{q,n}} \right)^{2}$$

$$\geq (2L-2) \sum_{i \in \mathcal{N}} S^{i} \alpha^{2S^{i}(L-1) + S_{1}^{i} + 2S_{3}^{i} - 1} \beta^{S_{1}^{i} + S_{2}^{i} + 1}$$

$$\geq (2L-2) \sum_{i \in \mathcal{N}} S^{i} \alpha^{2SL-1} \beta^{S+1} \qquad (D4a)$$

$$\geq |\mathcal{N}| (2L-2) \alpha^{2SL-1} \beta^{S+1}. \qquad (D4b)$$

Here, Eq. (D4a) is due to Eq. (D1), and Eq. (D4b) is due to the non-triviality of each term in the general Hamiltonian of Eq. (3), that is, $S^{i} \geq 1$, for all $i \in \mathcal{N}$.

Next, we calculate the second summation in Eq. (D2). Note that

$$\mathbb{E}\left(\frac{\partial C_{i}}{\partial \theta_{q,n}} \frac{\partial C_{j}}{\partial \theta_{q,n}}\right) = \mathbb{E}\left(\frac{\partial}{\partial \theta_{q,n}} \operatorname{Tr}\left[\boldsymbol{\sigma_{i}}\rho_{2L}\right] \frac{\partial}{\partial \theta_{q,n}} \operatorname{Tr}\left[\boldsymbol{\sigma_{j}}\rho_{2L}\right]\right). \tag{D5}$$

We first consider the case where $I_{S^i} \cap I_{S^j} = \emptyset$. Similar to obtaining Eqs. (C8a) and (C8b), we have

$$\mathbb{E}_{\boldsymbol{\theta}} \left(\frac{\partial C_{\boldsymbol{i}}}{\partial \theta_{a,n}} \frac{\partial C_{\boldsymbol{j}}}{\partial \theta_{a,n}} \right) = 0. \tag{D6}$$

Then we consider the case where $I_{S^i} \cap I_{S^j} \neq \emptyset$. Following the technique used for the case i+1=j and the form of Eq. (C13) in Appendix C, Eq. (D5) can be rewritten as a sum of non-negative terms

$$\mathbb{E}_{\boldsymbol{\theta}} \left(\frac{\partial C_{\boldsymbol{i}}}{\partial \theta_{q,n}} \frac{\partial C_{\boldsymbol{j}}}{\partial \theta_{q,n}} \right) = \sum_{k} c_{k} \operatorname{Tr} \left[\boldsymbol{\sigma}_{\boldsymbol{g}_{\boldsymbol{i}}^{k}} \rho_{0} \right] \operatorname{Tr} \left[\boldsymbol{\sigma}_{\boldsymbol{g}_{\boldsymbol{j}}^{k}} \rho_{0} \right] \geq 0,$$
(D7)

where c_k denotes the positive coefficient, $\sigma_{g_i^k}$ and $\sigma_{g_j^k}$ denote the N-qubit Pauli strings generated from σ_i and σ_j , respectively. The non-negativity is owing to the chosen initial state $\rho_0 = |0\rangle\langle 0|$.

Therefore, the second summation in Eq. (D2) is non-negative, i.e.,

$$\sum_{i \neq j \in \mathcal{N}} \sum_{q=1}^{2L} \sum_{n=1}^{N} \mathbb{E} \left(\frac{\partial C_i}{\partial \theta_{q,n}} \frac{\partial C_j}{\partial \theta_{q,n}} \right) \ge 0.$$
 (D8)

Combining Eq. (D4b) and Eq. (D8), we have Eq. (8). Finally, we determine the hyperparameter a by maximizing the lower bound in Eq. (8) denoted by

$$G(S, L, a) \triangleq 2|\mathcal{N}|(L-1)\alpha^{2SL-1}\beta^{S+1}.$$

It can be verified that G(S, L, a) attains its maximum when a is chosen as the solution of the following equation

$$\frac{\sin 2a\pi}{2a\pi} = \frac{S(2L-1) - 2}{S(2L+1)},$$

and the solution a has the same scaling as $\frac{1}{\sqrt{L}}$, that is, $a \in \Theta(\frac{1}{\sqrt{L}})$. Moreover, with the selected a, we have

$$G(S, L, a) \ge 2|\mathcal{N}| \left(\frac{S+1}{eS}\right)^{S+1} \frac{L-1}{(2L+1)^{S+1}},$$

which is obtained by the fact that the function $\left[\frac{2SL-1}{S(2L+1)}\right]^{2SL-1}$ decreases monotonically with L and converges to $\frac{1}{e^{S+1}}$, when $S \geq 1$.

Appendix E: Proof of Theorem III.3

Proof. Let us first prove Eq. (11) concerning the average of the partial derivative of the cost function with respect to $\theta_{q,n}$.

For the warm-up Hamiltonian of Eq. (4),

$$\underset{\boldsymbol{\theta}}{\mathbb{E}} \, \partial_{\theta_{q,n}} C = \sum_{i=1}^{N-1} \underset{\boldsymbol{\theta}}{\mathbb{E}} \, \partial_{\theta_{q,n}} C_i,$$

where $C_i = \text{Tr} \left[Z_i Z_{i+1} U(\boldsymbol{\theta}) \rho U^{\dagger}(\boldsymbol{\theta}) \right]$. To proceed, assume that $\theta_{q,n}$ lies in the *l*th block. Then, we have

$$\mathbb{E} \, \partial_{\theta_{q,n}} C_{i} = \mathbb{E} \, \partial_{\theta_{q,n}} \operatorname{Tr} \left[Z_{i} Z_{i+1} \rho_{2L} \right] \\
= \gamma^{2} \, \mathbb{E} \, \partial_{\theta_{q,n}} \operatorname{Tr} \left[Z_{i} Z_{i+1} \rho_{2L-1} \right] \qquad (E1a) \\
= \gamma^{4} \, \mathbb{E} \, \partial_{\theta_{q,n}} \operatorname{Tr} \left[\operatorname{CZ}_{L}^{\dagger} Z_{i} Z_{i+1} \operatorname{CZ}_{L} \rho_{2L-2} \right] \\
= \gamma^{4} \, \mathbb{E} \, \partial_{\theta_{q,n}} \operatorname{Tr} \left[\operatorname{Z}_{i} Z_{i+1} \rho_{2L-2} \right] \qquad (E1b) \\
= \gamma^{4} \, \mathbb{E} \, \partial_{\theta_{q,n}} \operatorname{Tr} \left[Z_{i} Z_{i+1} \rho_{2L-2} \right] \qquad (E1c) \\
= \gamma^{4(L-l)} \, \mathbb{E} \, \partial_{\theta_{q,n}} \operatorname{Tr} \left[Z_{i} Z_{i+1} \rho_{2l} \right]. \qquad (E1d)$$

Here, the appearance of γ^2 in Eq. (E1a) is due to taking the expectations over $\theta_{2L,i}$ and $\theta_{2L,i+1}$ by employing Eq. (B1) and taking the expectations over the other N-2 parameters in θ_{2L} by utilizing Eq. (B3). Following the same reasoning, Eq. (E1b) is derived. In addition, Eq. (E1c) is due to Lemma B.6. Eqs. (E1a)-(E1c) comprise a complete calculation for the Lth block in Fig. 1(a). For the following L-l-1 blocks, we repeat the same procedures and obtain Eq. (E1d).

Now we proceed upon the index n. For $n \notin \{i, i+1\}$, from Eq. (B4), we have

$$\underset{\theta_{q,n}}{\mathbb{E}} \partial_{\theta_{q,n}} \operatorname{Tr} \left[Z_i Z_{i+1} \rho_q \right] = 0,$$

which results in $\underset{\boldsymbol{\theta}}{\mathbb{E}} \partial_{\theta_{q,n}} C = 0$.

For $n \in \{i, i+1\}$, we first consider the case where q=2l. Note that by employing Eq. (B2) for $\theta_{q,n}$, we have

$$\mathbb{E}_{\theta_{2l}} \partial_{\theta_{2l,n}} \text{Tr} [Z_i Z_{i+1} \rho_{2l}]
= \begin{cases}
-\gamma^2 \text{Tr} [X_i Z_{i+1} \rho_{2l-1}], & n = i \\
-\gamma^2 \text{Tr} [Z_i X_{i+1} \rho_{2l-1}], & n = i + 1.
\end{cases} (E2)$$

Moreover, by employing Eq. (B1), we have

$$\begin{cases} \mathbb{E} \operatorname{Tr} \left[X_i Z_{i+1} \rho_{2l-1} \right] = \gamma \operatorname{Tr} \left[\operatorname{CZ}_l^{\dagger} X_i Z_{i+1} \operatorname{CZ}_l \rho_{2l-2} \right], \\ n = i, \\ \mathbb{E} \operatorname{Tr} \left[Z_i X_{i+1} \rho_{2l-1} \right] = \gamma \operatorname{Tr} \left[\operatorname{CZ}_l^{\dagger} Z_i X_{i+1} \operatorname{CZ}_l \rho_{2l-2} \right], \\ n = i+1. \end{cases}$$
(E3)

Combining Eq. (E2) and Eq. (E3), we obtain

$$\mathbb{E}_{\boldsymbol{\theta}_{2l-1}} \mathbb{E}_{\boldsymbol{\theta}_{2l}} \partial_{\boldsymbol{\theta}_{2l,n}} \operatorname{Tr} \left[Z_i Z_{i+1} \rho_{2l} \right] \\
= \begin{cases}
-\gamma^3 \operatorname{Tr} \left[\operatorname{CZ}_l^{\dagger} X_i Z_{i+1} \operatorname{CZ}_l \rho_{2l-2} \right], & n = i \\
-\gamma^3 \operatorname{Tr} \left[\operatorname{CZ}_l^{\dagger} Z_i X_{i+1} \operatorname{CZ}_l \rho_{2l-2} \right], & n = i+1.
\end{cases} (E4)$$

Similarly, for $n \in \{i, i+1\}$ and q = 2l - 1, we have

$$\mathbb{E}_{\boldsymbol{\theta}_{2l-1}} \mathbb{E}_{\boldsymbol{\theta}_{2l}} \partial_{\theta_{2l-1,n}} \operatorname{Tr} \left[Z_{i} Z_{i+1} \rho_{2l} \right]
= \gamma^{2} \mathbb{E}_{\boldsymbol{\theta}_{2l-1}} \partial_{\theta_{2l-1,n}} \operatorname{Tr} \left[Z_{i} Z_{i+1} \rho_{2l-1} \right]
= \begin{cases} \gamma^{4} \operatorname{Tr} \left[\operatorname{CZ}_{l}^{\dagger} Y_{i} Z_{i+1} \operatorname{CZ}_{l} \rho_{2l-2} \right], & n = i \\ \gamma^{4} \operatorname{Tr} \left[\operatorname{CZ}_{l}^{\dagger} Z_{i} Y_{i+1} \operatorname{CZ}_{l} \rho_{2l-2} \right], & n = i + 1. \end{cases}$$
(E5)

According to Lemma B.6, after applying the lth entanglement layer, the generated observables in Eqs. (E4) and (E5) are all N-qubit Pauli strings with the nth tensor component unchanged and being either Pauli X or Pauli Y.

Subsequently, from Eqs. (B1) and (B3), taking the expectations over $\theta_{q-1}, \ldots, \theta_1$ does not change the observables any longer. Moreover, applying the entanglement layers does not change the *n*th tensor component of the observables in Eqs. (E4) and (E5), which is either Pauli X or Pauli Y. Thus, for $n \in \{i, i+1\}$, we have

$$\underset{\boldsymbol{\theta}_{[2l]}}{\mathbb{E}} \partial_{\theta_{q,n}} \operatorname{Tr} \left[Z_i Z_{i+1} \rho_{2l} \right] = c \operatorname{Tr} \left[\boldsymbol{\sigma}_{\boldsymbol{g}_i} \rho_0 \right], \quad (E6)$$

where c is a positive coefficient, σ_{g_i} denotes the final Pauli string generated from $Z_i Z_{i+1}$, whose nth tensor component is Pauli X for q=2l and Pauli Y for q=2l-1. Moreover, with the choice of $\rho_0=|0\rangle\langle 0|$, Eq. (E6) is equal to zero, which results in $\mathbb{E} \frac{\partial_{\theta_{q,n}} C}{\partial \theta_{q,n} C}=0$.

Therefore, we have proved Eq. (11). The proof of Eqs. (12)-(17) can be straightforwardly derived from the proof in Appendix C. \Box

Appendix F: Proof of Theorem III.4

Proof. The proof of Eqs. (18) and (21) can be straightforwardly derived from the proof in Appendix D. We now focus on proving Eq. (19) when the number of the elements in vector \boldsymbol{i} belonging to $\{1,2\}$ is not equal to 1 for all $\boldsymbol{i} \in \mathcal{N}$.

Following the notation in Appendix D, we restate Eq. (19). Specifically, if $S_1^{\boldsymbol{i}} + S_2^{\boldsymbol{i}} \neq 1$ for all $\boldsymbol{i} \in \mathcal{N}$, for an arbitrary trainable parameter $\theta_{q,n}$,

$$\underset{\boldsymbol{\theta}}{\mathbb{E}} \, \partial_{\theta_{q,n}} C = \sum_{\boldsymbol{i} \in \mathcal{N}} \underset{\boldsymbol{\theta}}{\mathbb{E}} \, \partial_{\theta_{q,n}} C_{\boldsymbol{i}} = 0, \tag{F1}$$

where $C_i = \text{Tr} \left[\boldsymbol{\sigma}_i U(\boldsymbol{\theta}) \rho U^{\dagger}(\boldsymbol{\theta}) \right]$. To prove it, we assume that $\theta_{q,n}$ lies in the *l*th block.

First, if $S_1^i + S_2^i = 0$, we can directly generalize the proof in Appendix E to obtain

$$\underset{\boldsymbol{\theta}}{\mathbb{E}} \partial_{\theta_{q,n}} C_{\boldsymbol{i}} = 0. \tag{F2}$$

Next, if $S_1^{\boldsymbol{i}} + S_2^{\boldsymbol{i}} \geq 2$, note that

$$\mathbb{E}_{\boldsymbol{\theta}} \partial_{\theta_{q,n}} C_{\boldsymbol{i}} = \mathbb{E}_{\boldsymbol{\theta}_{[2L]}} \partial_{\theta_{q,n}} \operatorname{Tr} \left[\boldsymbol{\sigma}_{\boldsymbol{i}} \rho_{2L} \right] \\
= \gamma^{S_{1}^{i} + S_{3}^{i}} \mathbb{E}_{\boldsymbol{\theta}_{[2L-1]}} \partial_{\theta_{q,n}} \operatorname{Tr} \left[\boldsymbol{\sigma}_{\boldsymbol{i}} \rho_{2L-1} \right] \qquad (F3a) \\
= \gamma^{S^{i} + S_{3}^{i}} \mathbb{E}_{\boldsymbol{\theta}_{[2L-2]}} \partial_{\theta_{q,n}} \operatorname{Tr} \left[\operatorname{CZ}_{L}^{\dagger} \boldsymbol{\sigma}_{\boldsymbol{i}} \operatorname{CZ}_{L} \rho_{2L-2} \right] \\
\qquad \qquad (F3b) \\
= \gamma^{(S^{i} + S_{3}^{i})(L-l)} \mathbb{E}_{\boldsymbol{\theta}_{[2l]}} \partial_{\theta_{q,n}} \operatorname{Tr} \left[\boldsymbol{\sigma}_{\boldsymbol{g}_{i,2l}} \rho_{2l} \right]. \quad (F3c)$$

Here, Eqs. (F3a) and (F3b) are derived from the same reasoning as Eqs. (E1a) and (E1b), respectively. According to Lemma B.6, after applying the entanglement layer in Eq. (F3b), the position set of the tensor components being X or Y does not change, being equal to $I_{S_1^i} \cup I_{S_2^i}$. Then we repeat the above procedures for the following L-l-1 blocks and obtain Eq. (F3c), where $\sigma_{g_{i,2l}}$ denotes the generated observable after calculating the last L-l blocks with the invariant set $I_{S_1^{g_{i,2l}}} \cup I_{S_2^{g_{i,2l}}} = I_{S_1^i} \cup I_{S_2^i}$. By now, $S_1^{g_{i,2l}} + S_2^{g_{i,2l}} = S_1^i + S_2^i \geq 2$.

For the lth block where $\theta_{q,n}$ lies, from Lemma B.2, when taking the expectations over $\boldsymbol{\theta}_{2l}$ and $\boldsymbol{\theta}_{2l-1}$, the number of the tensor components being X or Y changes, which either increases or decreases by at most 1. In fact, the possible change only happens when employing Eq. (B2). Moreover, according to Lemma B.6, after calculating the lth block, we have

$$S_1^{g_{i,2(l-1)}} + S_2^{g_{i,2(l-1)}} \ge S_1^i + S_2^i - 1 \ge 1.$$

During the calculations of the expectations over $\theta_{[2(l-1)]}$, from Lemmas B.2 and B.6, the number of the tensor components being X or Y does not change any longer. Since

$$\mathbb{E}_{\mathbf{0}} \partial_{\theta_{q,n}} C_{\mathbf{i}} \propto \operatorname{Tr} \left[\boldsymbol{\sigma}_{\boldsymbol{g}_{\mathbf{i},0}} \rho_0 \right],$$

and at least one of the tensor components in $\sigma_{g_{i,0}}$ is X or Y, with the selected $\rho_0 = |0\rangle\langle 0|$, we have

$$\underset{\boldsymbol{\theta}}{\mathbb{E}} \, \partial_{\theta_{q,n}} C_{\boldsymbol{i}} = 0. \tag{F4}$$

Thus, Eq. (19) is proved and so is Eq. (20).

ACKNOWLEDGMENTS

B. Q. acknowledges the support of the National Natural Science Foundation of China (No. 61833010), and D. D. acknowledges the support of the Australian Research Council's Future Fellowship funding scheme under project FT220100656 and the U.S. Office of Naval Research Global under Grant No. N62909-19-1-2129.

- [1] J. Preskill, Quantum computing in the NISQ era and beyond, Quantum 2, 79 (2018).
- [2] M. Ippoliti, K. Kechedzhi, R. Moessner, S. Sondhi, and V. Khemani, Many-body physics in the NISQ era: Quantum programming a discrete time crystal, PRX Quantum 2, 030346 (2021).
- [3] K. Bharti, A. Cervera-Lierta, T. H. Kyaw, T. Haug, S. Alperin-Lea, A. Anand, M. Degroote, H. Heimonen, J. S. Kottmann, T. Menke, W.-K. Mok, S. Sim, L.-C. Kwek, and A. Aspuru-Guzik, Noisy intermediate-scale quantum algorithms, Rev. Mod. Phys. 94, 015004 (2022).
- [4] F. Arute, K. Arya, R. Babbush, D. Bacon, J. C. Bardin, R. Barends, R. Biswas, S. Boixo, F. G. Brandao, D. A. Buell, et al., Quantum supremacy using a programmable superconducting processor, Nature 574, 505 (2019).
- [5] H.-S. Zhong, H. Wang, Y.-H. Deng, M.-C. Chen, L.-C. Peng, Y.-H. Luo, J. Qin, D. Wu, X. Ding, Y. Hu, P. Hu, X.-Y. Yang, W.-J. Zhang, H. Li, Y. Li, X. Jiang, L. Gan, G. Yang, L. You, Z. Wang, L. Li, N.-L. Liu, C.-Y. Lu, and J.-W. Pan, Quantum computational advantage using photons, Science 370, 1460 (2020).
- [6] I. H. Deutsch, Harnessing the power of the second quantum revolution, PRX Quantum 1, 020101 (2020).
- [7] H.-Y. Huang, M. Broughton, M. Mohseni, R. Babbush, S. Boixo, H. Neven, and J. R. McClean, Power of data in quantum machine learning, Nat. Commun. 12, 1 (2021).
- [8] H.-Y. Huang, M. Broughton, J. Cotler, S. Chen, J. Li, M. Mohseni, H. Neven, R. Babbush, R. Kueng, J. Preskill, and J. R. McClean, Quantum advantage in learning from experiments, Science 376, 1182 (2021).
- [9] Y. Du, M.-H. Hsieh, T. Liu, S. You, and D. Tao, Learnability of quantum neural networks, PRX Quantum 2, 040337 (2021).
- [10] X. Wang, Y. Du, Y. Luo, and D. Tao, Towards understanding the power of quantum kernels in the NISQ era, Quantum 5, 531 (2021).
- [11] J. M. Kübler, S. Buchholz, and B. Schölkopf, The inductive bias of quantum kernels, in *Advances in Neural Information Processing Systems*, edited by A. Beygelzimer, Y. Dauphin, P. Liang, and J. W. Vaughan (Curran Associates, Inc., 2021) pp. 12661–12673.
- [12] G. E. Crooks, Performance of the quantum approximate optimization algorithm on the maximum cut problem, arXiv:1811.08419 (2018).
- [13] E. Farhi and A. W. Harrow, Quantum supremacy through the quantum approximate optimization algorithm, arXiv:1602.07674 (2016).
- [14] H. Yamasaki, S. Subramanian, S. Sonoda, and M. Koashi, Learning with optimized random features: Exponential speedup by quantum machine learning without sparsity and low-rank assumptions, in *Advances in Neural Information Processing Systems*, Vol. 33, edited by H. Larochelle, M. Ranzato, R. Hadsell, M. Balcan, and H. Lin (Curran Associates, Inc., 2020) pp. 13674–13687.
- [15] S. Jerbi, C. Gyurik, S. C. Marshall, H. J. Briegel, and V. Dunjko, Parametrized quantum policies for reinforcement learning, in *Advances in Neural Information Processing Systems*, edited by A. Beygelzimer, Y. Dauphin, P. Liang, and J. W. Vaughan (Curran Associates, Inc., 2021) pp. 28362–28375.
- [16] C.-N. Chou, P. J. Love, J. S. Sandhu, and J. Shi, Limi-

- tations of local quantum algorithms on random Max-k-XOR and beyond, arXiv:2108.06049 (2021).
- [17] J. R. McClean, J. Romero, R. Babbush, and A. Aspuru-Guzik, The theory of variational hybrid quantum-classical algorithms, New J. Phys. 18, 023023 (2016).
- [18] M. Cerezo, A. Arrasmith, R. Babbush, S. C. Benjamin, S. Endo, K. Fujii, J. R. McClean, K. Mitarai, X. Yuan, L. Cincio, et al., Variational quantum algorithms, Nat. Rev. Phys. 3, 625 (2021).
- [19] J. Liu, F. Tacchino, J. R. Glick, L. Jiang, and A. Mezzacapo, Representation learning via quantum neural tangent kernels, PRX Quantum 3, 030323 (2022).
- [20] S. Jerbi, L. J. Fiderer, H. Poulsen Nautrup, J. M. Kübler, H. J. Briegel, and V. Dunjko, Quantum machine learning beyond kernel methods, Nat. Commun. 14, 517 (2023).
- [21] M. Benedetti, E. Lloyd, S. Sack, and M. Fiorentini, Parameterized quantum circuits as machine learning models, Quantum Sci. Technol. 4, 043001 (2019).
- [22] D. P. Kingma and J. Ba, Adam: A method for stochastic optimization, arXiv:1412.6980 (2014).
- [23] D. Dong and I. R. Petersen, Quantum estimation, control and learning: Opportunities and challenges, Annual Reviews in Control 54, 243 (2022).
- [24] W. Lavrijsen, A. Tudor, J. Müller, C. Iancu, and W. De Jong, Classical optimizers for noisy intermediatescale quantum devices, in 2020 IEEE International Conference on Quantum Computing and Engineering (QCE) (2020) pp. 267–277.
- [25] A. Basheer, Y. Feng, C. Ferrie, and S. Li, Alternating layered variational quantum circuits can be classically optimized efficiently using classical shadows, arXiv:2208.11623 (2022).
- [26] R. Sweke, F. Wilde, J. Meyer, M. Schuld, P. K. Fährmann, B. Meynard-Piganeau, and J. Eisert, Stochastic gradient descent for hybrid quantum-classical optimization, Quantum 4, 314 (2020).
- [27] K. Temme, S. Bravyi, and J. M. Gambetta, Error mitigation for short-depth quantum circuits, Phys. Rev. Lett. 119, 180509 (2017).
- [28] S. Endo, S. C. Benjamin, and Y. Li, Practical quantum error mitigation for near-future applications, Phys. Rev. X 8, 031027 (2018).
- [29] S. Endo, Z. Cai, S. C. Benjamin, and X. Yuan, Hybrid quantum-classical algorithms and quantum error mitigation, J. Phys. Soc. Jpn. 90, 032001 (2021).
- [30] Z. Cai, R. Babbush, S. C. Benjamin, S. Endo, W. J. Huggins, Y. Li, J. R. McClean, and T. E. O'Brien, Quantum error mitigation, arXiv:2210.00921 (2022).
- [31] A. Strikis, D. Qin, Y. Chen, S. C. Benjamin, and Y. Li, Learning-based quantum error mitigation, PRX Quantum 2, 040330 (2021).
- [32] A. Peruzzo, J. McClean, P. Shadbolt, M.-H. Yung, X.-Q. Zhou, P. J. Love, A. Aspuru-Guzik, and J. L. O'brien, A variational eigenvalue solver on a photonic quantum processor, Nat. Commun. 5, 1 (2014).
- [33] M. Ostaszewski, L. M. Trenkwalder, W. Masarczyk, E. Scerri, and V. Dunjko, Reinforcement learning for optimization of variational quantum circuit architectures, in *Advances in Neural Information Processing Sys*tems, Vol. 34, edited by M. Ranzato, A. Beygelzimer, Y. Dauphin, P. Liang, and J. W. Vaughan (Curran As-

- sociates, Inc., 2021) pp. 18182-18194.
- [34] A. Kandala, A. Mezzacapo, K. Temme, M. Takita, M. Brink, J. M. Chow, and J. M. Gambetta, Hardwareefficient variational quantum eigensolver for small molecules and quantum magnets, Nature 549, 242 (2017).
- [35] J. Tilly, H. Chen, S. Cao, D. Picozzi, K. Setia, Y. Li, E. Grant, L. Wossnig, I. Rungger, G. H. Booth, et al., The variational quantum eigensolver: A review of methods and best practices, Phys. Rep. 986, 1 (2022).
- [36] E. Farhi, J. Goldstone, and S. Gutmann, A quantum approximate optimization algorithm, arXiv:1411.4028 (2014).
- [37] Z. Wang, S. Hadfield, Z. Jiang, and E. G. Rieffel, Quantum approximate optimization algorithm for MaxCut: A fermionic view, Phys. Rev. A 97, 022304 (2018).
- [38] S. Hadfield, Z. Wang, E. G. Rieffel, B. O'Gorman, D. Venturelli, and R. Biswas, Quantum approximate optimization with hard and soft constraints, in *Proceedings* of the Second International Workshop on Post Moores Era Supercomputing (Association for Computing Machinery, 2017) p. 15–21.
- [39] L. Zhou, S.-T. Wang, S. Choi, H. Pichler, and M. D. Lukin, Quantum approximate optimization algorithm: Performance, mechanism, and implementation on near-term devices, Phys. Rev. X 10, 021067 (2020).
- [40] E. Altman, K. R. Brown, G. Carleo, L. D. Carr, E. Demler, C. Chin, B. DeMarco, S. E. Economou, M. A. Eriksson, K.-M. C. Fu, M. Greiner, K. R. Hazzard, R. G. Hulet, A. J. Kollár, B. L. Lev, M. D. Lukin, R. Ma, X. Mi, S. Misra, C. Monroe, K. Murch, Z. Nazario, K.-K. Ni, A. C. Potter, P. Roushan, M. Saffman, M. Schleier-Smith, I. Siddiqi, R. Simmonds, M. Singh, I. Spielman, K. Temme, D. S. Weiss, J. Vučković, V. Vuletić, J. Ye, and M. Zwierlein, Quantum simulators: Architectures and opportunities, PRX Quantum 2, 017003 (2021).
- [41] Y. Li and S. C. Benjamin, Efficient variational quantum simulator incorporating active error minimization, Phys. Rev. X 7, 021050 (2017).
- [42] X. Yuan, S. Endo, Q. Zhao, Y. Li, and S. C. Benjamin, Theory of variational quantum simulation, Quantum 3, 191 (2019).
- [43] K. Bharti and T. Haug, Quantum-assisted simulator, Phys. Rev. A 104, 042418 (2021).
- [44] J. Biamonte, P. Wittek, N. Pancotti, P. Rebentrost, N. Wiebe, and S. Lloyd, Quantum machine learning, Nature 549, 195 (2017).
- [45] V. Dunjko and H. J. Briegel, Machine learning & artificial intelligence in the quantum domain: a review of recent progress, Rep. Prog. Phys. 81, 074001 (2018).
- [46] J. Liu, K. Najafi, K. Sharma, F. Tacchino, L. Jiang, and A. Mezzacapo, An analytic theory for the dynamics of wide quantum neural networks, arXiv:2203.16711 (2022).
- [47] W. Li and D.-L. Deng, Recent advances for quantum classifiers, Sci. China Phys. Mech. Astron. 65, 1 (2022).
- [48] E. Farhi and H. Neven, Classification with quantum neural networks on near term processors, arXiv:1802.06002 (2018).
- [49] M. Schuld, A. Bocharov, K. M. Svore, and N. Wiebe, Circuit-centric quantum classifiers, Phys. Rev. A 101, 032308 (2020).
- [50] I. Cong, S. Choi, and M. D. Lukin, Quantum convolutional neural networks, Nat. Phys. 15, 1273 (2019).

- [51] I. Kerenidis, J. Landman, and A. Prakash, Quantum algorithms for deep convolutional neural networks, in *International Conference on Learning Representations* (2020).
- [52] S. Chakrabarti, H. Yiming, T. Li, S. Feizi, and X. Wu, Quantum wasserstein generative adversarial networks, in *Advances in Neural Information Processing Systems*, Vol. 32, edited by H. Wallach, H. Larochelle, A. Beygelzimer, F. d'Alché-Buc, E. Fox, and R. Garnett (Curran Associates, Inc., 2019).
- [53] J. Romero, J. P. Olson, and A. Aspuru-Guzik, Quantum autoencoders for efficient compression of quantum data, Quantum Sci. Technol. 2, 045001 (2017).
- [54] J. Romero and A. Aspuru-Guzik, Variational quantum generators: Generative adversarial quantum machine learning for continuous distributions, Advanced Quantum Technologies 4, 2000003 (2021).
- [55] E. Perrier, D. Tao, and C. Ferrie, Quantum geometric machine learning for quantum circuits and control, New J. Phys. 22, 103056 (2020).
- [56] R.-B. Wu, X. Cao, P. Xie, and Y.-x. Liu, End-to-end quantum machine learning implemented with controlled quantum dynamics, Phys. Rev. Appl. 14, 064020 (2020).
- [57] K. Bharti and T. Haug, Iterative quantum-assisted eigensolver, Phys. Rev. A 104, L050401 (2021).
- [58] S. Khatri, R. LaRose, A. Poremba, L. Cincio, A. T. Sorn-borger, and P. J. Coles, Quantum-assisted quantum compiling, Quantum 3, 140 (2019).
- [59] C. Bravo-Prieto, D. García-Martín, and J. I. Latorre, Quantum singular value decomposer, Phys. Rev. A 101, 062310 (2020).
- [60] H.-Y. Huang, K. Bharti, and P. Rebentrost, Near-term quantum algorithms for linear systems of equations with regression loss functions, New J. Phys. 23, 113021 (2021).
- [61] A. H. Karamlou, W. A. Simon, A. Katabarwa, T. L. Scholten, B. Peropadre, and Y. Cao, Analyzing the performance of variational quantum factoring on a superconducting quantum processor, npj Quantum Inf. 7, 1 (2021).
- [62] J. R. McClean, S. Boixo, V. N. Smelyanskiy, R. Babbush, and H. Neven, Barren plateaus in quantum neural network training landscapes, Nat. Commun. 9, 1 (2018).
- [63] T. Haug, K. Bharti, and M. Kim, Capacity and quantum geometry of parametrized quantum circuits, PRX Quantum 2, 040309 (2021).
- [64] C. Zhao and X.-S. Gao, Analyzing the barren plateau phenomenon in training quantum neural networks with the ZX-calculus, Quantum 5, 466 (2021).
- [65] M. Cerezo, A. Sone, T. Volkoff, L. Cincio, and P. J. Coles, Cost function dependent barren plateaus in shallow parametrized quantum circuits, Nat. Commun. 12, 1 (2021).
- [66] Z. Liu, L.-W. Yu, L.-M. Duan, and D.-L. Deng, Presence and absence of barren plateaus in tensor-network based machine learning, Phys. Rev. Lett. 129, 270501 (2022).
- [67] Z. Holmes, K. Sharma, M. Cerezo, and P. J. Coles, Connecting ansatz expressibility to gradient magnitudes and barren plateaus, PRX Quantum 3, 010313 (2022).
- [68] C. O. Marrero, M. Kieferová, and N. Wiebe, Entanglement-induced barren plateaus, PRX Quantum 2, 040316 (2021).
- [69] K. Sharma, M. Cerezo, L. Cincio, and P. J. Coles, Trainability of dissipative perceptron-based quantum neural networks, Phys. Rev. Lett. 128, 180505 (2022).

- [70] S. Wang, E. Fontana, M. Cerezo, K. Sharma, A. Sone, L. Cincio, and P. J. Coles, Noise-induced barren plateaus in variational quantum algorithms, Nat. Commun. 12, 1 (2021).
- [71] A. Arrasmith, M. Cerezo, P. Czarnik, L. Cincio, and P. J. Coles, Effect of barren plateaus on gradient-free optimization, Quantum 5, 558 (2021).
- [72] E. R. Anschuetz and B. T. Kiani, Quantum variational algorithms are swamped with traps, Nat. Commun. 13, 7760 (2022).
- [73] X. You and X. Wu, Exponentially many local minima in quantum neural networks, in *Proceedings of the 38th International Conference on Machine Learning (ICML 2021)* (2021) pp. 12144–12155.
- [74] L. Bittel and M. Kliesch, Training variational quantum algorithms is NP-hard, Phys. Rev. Lett. 127, 120502 (2021).
- [75] X. Ge, R.-B. Wu, and H. Rabitz, The optimization landscape of hybrid quantum-classical algorithms: From quantum control to NISQ applications, Annual Reviews in Control 54, 314 (2022).
- [76] Y.-Y. Shi, L.-M. Duan, and G. Vidal, Classical simulation of quantum many-body systems with a tree tensor network, Phys. Rev. A 74, 022320 (2006).
- [77] E. Grant, M. Benedetti, S. Cao, A. Hallam, J. Lockhart, V. Stojevic, A. G. Green, and S. Severini, Hierarchical quantum classifiers, npj Quantum Inf. 4, 1 (2018).
- [78] K. Zhang, M.-H. Hsieh, L. Liu, and D. Tao, Toward trainability of quantum neural networks, arXiv:2011.06258 (2020).
- [79] A. Pesah, M. Cerezo, S. Wang, T. Volkoff, A. T. Sorn-borger, and P. J. Coles, Absence of barren plateaus in quantum convolutional neural networks, Phys. Rev. X 11, 041011 (2021).
- [80] R. Wiersema, C. Zhou, Y. de Sereville, J. F. Carrasquilla, Y. B. Kim, and H. Yuen, Exploring entanglement and optimization within the Hamiltonian variational ansatz, PRX Quantum 1, 020319 (2020).
- [81] S. Hadfield, Z. Wang, B. O'gorman, E. G. Rieffel, D. Venturelli, and R. Biswas, From the quantum approximate optimization algorithm to a quantum alternating operator ansatz, Algorithms 12, 34 (2019).
- [82] D. A. Fedorov, B. Peng, N. Govind, and Y. Alexeev, VQE method: A short survey and recent developments, Materials Theory 6, 1 (2022).
- [83] Y. Du, T. Huang, S. You, M.-H. Hsieh, and D. Tao, Quantum circuit architecture search for variational quan-

- tum algorithms, npj Quantum Inf. 8, 1 (2022).
- [84] A. Skolik, J. R. McClean, M. Mohseni, P. van der Smagt, and M. Leib, Layerwise learning for quantum neural networks, Quantum Mach. Intell. 3, 1 (2021).
- [85] E. Campos, D. Rabinovich, V. Akshay, and J. Biamonte, Training saturation in layerwise quantum approximate optimization, Phys. Rev. A 104, L030401 (2021).
- [86] O. Lockwood, Optimizing quantum variational circuits with deep reinforcement learning, arXiv:2109.03188 (2021).
- [87] E. Grant, L. Wossnig, M. Ostaszewski, and M. Benedetti, An initialization strategy for addressing barren plateaus in parametrized quantum circuits, Quantum 3, 214 (2019).
- [88] T. Volkoff and P. J. Coles, Large gradients via correlation in random parameterized quantum circuits, Quantum Sci. Technol. 6, 025008 (2021).
- [89] A. Rad, A. Seif, and N. M. Linke, Surviving the barren plateau in variational quantum circuits with Bayesian learning initialization, arXiv:2203.02464 (2022).
- [90] K. Zhang, L. Liu, M.-H. Hsieh, and D. Tao, Escaping from the barren plateau via gaussian initializations in deep variational quantum circuits, in *Advances in Neu*ral *Information Processing Systems*, edited by A. H. Oh, A. Agarwal, D. Belgrave, and K. Cho (2022).
- [91] H. A. Rabitz, M. M. Hsieh, and C. M. Rosenthal, Quantum optimally controlled transition landscapes, Science 303, 1998 (2004).
- [92] B. T. Kiani, S. Lloyd, and R. Maity, Learning unitaries by gradient descent, arXiv:2001.11897 (2020).
- [93] E. R. Anschuetz, Critical points in quantum generative models, in *International Conference on Learning Repre*sentations (2022).
- [94] M. Larocca, N. Ju, D. García-Martín, P. J. Coles, and M. Cerezo, Theory of overparametrization in quantum neural networks, arXiv:2109.11676 (2021).
- [95] J. Romero, R. Babbush, J. R. McClean, C. Hempel, P. J. Love, and A. Aspuru-Guzik, Strategies for quantum computing molecular energies using the unitary coupled cluster ansatz, Quantum Sci. Technol. 4, 014008 (2018).
- [96] K. Mitarai, M. Negoro, M. Kitagawa, and K. Fujii, Quantum circuit learning, Phys. Rev. A 98, 032309 (2018).
- [97] M. Schuld, V. Bergholm, C. Gogolin, J. Izaac, and N. Killoran, Evaluating analytic gradients on quantum hardware, Phys. Rev. A 99, 032331 (2019).
- [98] I. Loshchilov and F. Hutter, Decoupled weight decay regularization, in *International Conference on Learning Representations* (2019).